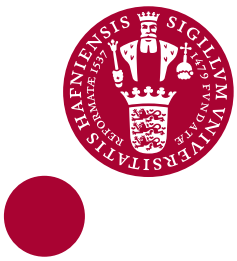

Alpha-synuclein aggregates activate calcium pump SERCA leading to calcium dysregulation

Betzer, Cristine; Lassen, Louise Berkhoudt; Olsen, Anders; Kofoed, Rikke Hahn; Reimer, Lasse; Gregersen, Emil; Zheng, Jin; Calì, Tito; Gai, Wei Ping; Chen, Tong; Moeller, Arne; Brini, Marisa; Fu, Yuhong; Halliday, Glenda; Brudek, Tomasz; Aznar, Susana; Pakkenberg, Bente; Andersen, Jens Peter; Jensen, Poul Henning

Published in:
EMBO Reports

DOI:
10.15252/embr.201744617

Publication date:
2018

Document version
Publisher's PDF, also known as Version of record

Published online: March 29, 2018

Article

TRANSPARENT PROCESS OPEN ACCESS

EMBO reports

Alpha-synuclein aggregates activate calcium pump SERCA leading to calcium dysregulation

Cristine Betzer[1,2], Louise Berkhoudt Lassen[1,2], Anders Olsen[3], Rikke Hahn Kofoed[1,2], Lasse Reimer[1,2], Emil Gregersen[1,2], Jin Zheng[1,2], Tito Calì[4], Wei-Ping Gai[5], Tong Chen[6], Arne Moeller[1,7], Marisa Brini[8], Yuhong Fu[9], Glenda Halliday[9], Tomasz Brudek[10], Susana Aznar[10], Bente Pakkenberg[10], Jens Peter Andersen[2] & Poul Henning Jensen[1,2,*]

Abstract

Aggregation of α-synuclein is a hallmark of Parkinson's disease and dementia with Lewy bodies. We here investigate the relationship between cytosolic Ca^{2+} and α-synuclein aggregation. Analyses of cell lines and primary culture models of α-synuclein cytopathology reveal an early phase with reduced cytosolic Ca^{2+} levels followed by a later Ca^{2+} increase. Aggregated but not monomeric α-synuclein binds to and activates SERCA *in vitro*, and proximity ligation assays confirm this interaction in cells. The SERCA inhibitor cyclopiazonic acid (CPA) normalises both the initial reduction and the later increase in cytosolic Ca^{2+}. CPA protects the cells against α-synuclein-aggregate stress and improves viability in cell models and in *Caenorhabditis elegans in vivo*. Proximity ligation assays also reveal an increased interaction between α-synuclein aggregates and SERCA in human brains affected by dementia with Lewy bodies. We conclude that α-synuclein aggregates bind SERCA and stimulate its activity. Reducing SERCA activity is neuroprotective, indicating that SERCA and down-stream processes may be therapeutic targets for treating α-synucleinopathies.

Keywords aggregation; alpha-synuclein; calcium; endoplasmic reticulum; SERCA

Subject Categories Membrane & Intracellular Transport; Molecular Biology of Disease; Neuroscience

DOI 10.15252/embr.201744617 | Received 10 June 2017 | Revised 13 February 2018 | Accepted 26 February 2018 | Published online 29 March 2018

EMBO Reports (2018) 19: e44617

Introduction

The small unfolded neuronal protein α-synuclein (AS) is closely linked to Parkinson's disease (PD). This is evidenced by the findings that autosomal-dominant familial PD can be caused by duplications and triplications of the normal *SNCA* gene encoding AS, by missense mutations causing exchange of single-amino acid residues (A30P, E46K, H50Q, G51D and A53T, A53E), and by variations in the SNCA gene, which represents the greatest genetic risk factor for sporadic PD. Aggregated amyloid-type fibrillar forms of AS accumulate in intra-neuronal Lewy body inclusions, which are the pathological hallmark of PD. Similar AS-containing intracellular inclusions also exist in other neurodegenerative diseases, so-called α-synucleinopathies, that besides PD are dominated by dementia with Lewy bodies (DLB) and multiple system atrophy (MSA). On the pathway from native protein to aggregated amyloid species, soluble oligomeric species are hypothesised to represent cytotoxic forms. The molecular mechanisms whereby AS aggregates contribute to the degeneration of neuronal populations are still unclear, but it has been proposed that they may be linked to perturbations of homeostatic mechanisms, for example proteostasis, mitochondrial functions, and direct toxic actions on membranes (reviewed in [1]).

Disturbances in brain Ca^{2+} regulation have recently been linked to PD because treatment of hypertension with antagonists of L-type Ca^{2+} CaV1 channels reduces the risk of PD [2–4] and the expression of CaV channels in the brain is changed in PD [4,5]. Average cytosolic Ca^{2+} concentrations are kept in the nM range, contrasting with the mM concentrations present outside cells and in the endoplasmic reticulum. The steep gradient makes Ca^{2+} an ideal signalling molecule because its cytosolic concentrations can be regulated precisely with spatio-temporal precision by opening of Ca^{2+} channels. Once

1 Danish Research Institute of Translational Neuroscience – DANDRITE, Aarhus University, Aarhus, Denmark
2 Department of Biomedicine, Aarhus University, Aarhus, Denmark
3 Department of Molecular Biology and Genetics, Aarhus University, Aarhus, Denmark
4 Department of Biomedical Sciences, University of Padova, Padova, Italy
5 Neuropathological Laboratory, Department of Medicine, Center for Neurological Diseases, University of Adelaide, Adelaide, SA, Australia
6 Department of Medical Biochemistry, School of Medicine, Flinders University, Bedford Park, SA, Australia
7 Department of Structural Biology, Max Plank Institute of Biophysics, Frankfurt, Germany
8 Department of Biology, University of Padova, Padova, Italy
9 Brain & Mind Centre, Sydney Medical School, The University of Sydney, Sydney, NSW, Australia
10 Research Laboratory for Stereology and Neuroscience, Bispebjerg-Frederiksberg Hospital, Copenhagen, Denmark
*Corresponding author. Tel: +45 28992056; E-mail: phj@biomed.au.dk

in the cytosol, Ca^{2+} has to be removed by active transporting pumps in ER, Golgi and the plasma membrane, by Na^{+}/Ca^{2+} exchanger in the plasma membrane, and by mitochondrial buffering. The mechanism whereby Ca^{2+} channel antagonists modulate the disease course of PD is still unknown, but it is hypothesised that the mechanism reduces the oxidant stress of dopaminergic neurons of substantia nigra that display an energy-consuming pacemaking firing pattern driven by Ca^{2+} influx via CaV1 channels [6]. How this localised effect in dopaminergic neurons is related to the progressive nature of PD remains unclear, but recent data indicate a complex interplay between AS, cytosolic Ca^{2+} and CaV1 channels in dopaminergic substantia nigra neurons [7]. Braak hypothesised that PD arises in the deep brainstem nuclei and spreads via the midbrain to neocortical regions [8]. This spreading pattern can be clinically observed in some patients, where REM sleep behaviour disorder (RBD) represents a prodromal phase of PD, and most PD patients develop cognitive impairment and dementia in their later phases due to involvement of neocortex.

Ca^{2+} deregulation has also been hypothesised as playing a general role in several neurodegenerative diseases like Alzheimer's disease and Huntington's disease. In these diseases, increased cytosolic Ca^{2+} represents a common theme which suggests the presence of mechanisms that lead to the influx of Ca^{2+} from extracellular space, endoplasmic reticulum and mitochondria as targets for therapeutic intervention [9].

We have previously demonstrated that AS aggregate-dependent degenerative processes are initiated at very early time points in cell models when no overt phenotypes are present [10]. In the present study, we investigated the temporal development of changes in cytosolic Ca^{2+} in cellular and neuronal models of AS aggregate-dependent degeneration. Surprisingly, we observed early reduction in cytosolic Ca^{2+} across models. This reduction was later followed by increased cytosolic Ca^{2+} when degeneration became apparent. Inhibitors of AS aggregation blocked both the early and late Ca^{2+} changes. This suggests activation of mechanisms whereby cytosolic Ca^{2+} is removed against large gradients. Co-immunoprecipitation experiments demonstrated that soluble and insoluble AS aggregates bind to the Ca^{2+} pump SERCA in contrast to monomers. SERCA is located in the endoplasmic reticulum. Their interaction was validated in cells using proximity ligation assays (PLA) where the antibody pair against SERCA and AS only produced a signal when the aggregation was not prevented. *In vitro* biochemical experiments demonstrate that AS aggregates activate the transmembrane Ca^{2+} pumping and ATP hydrolysis by SERCA. Counteracting the activation of SERCA in cells with the SERCA inhibitor cyclopiazonic acid (CPA) abrogated both the early reduction and later increase in cytosolic Ca^{2+} and protected cells and neurons against AS aggregate-dependent cell death. Treatment of AS-transgenic *Caenorhabditis elegans* with CPA protected the dopaminergic neurons against AS-dependent degeneration. Analyses of human brains by proximity ligation assay demonstrated the interaction between SERCA and aggregated AS in patients with DLB but not in controls. Moreover, SERCA was present in purified Lewy bodies from DLB patients and in glial cytoplasmic inclusions from MSA patients and SERCA copurified with insoluble AS in the detergent-insoluble fraction of MSA brain.

We hypothesise that a slow build-up of AS aggregates occurs within individual neurons during the process of disease spreading throughout the nervous system. We posit that the accumulating aggregates in the early stages activate SERCA and cause a reduction in cytosolic Ca^{2+}, triggering decisive pathophysiological changes and leading to ensuing cell death (Fig 8). Counteracting this early phase or its down-stream processes holds promise for increasing the vitality of the affected cells, thereby slowing and modifying the disease course.

Results

Neuronal Ca^{2+} homeostasis has been linked to PD pathogenesis by virtue of a reduced prevalence of sporadic PD among patients treated for hypertension with Ca^{2+}-antagonists [2,3] and genome-wide association studies linking the protective effect of caffeine against PD to the *GRIN2A* gene, which encodes a subunit of the *N*-methyl-D-aspartate receptor (NMDA)-activated Ca^{2+} channel [11,12]. Using the Ca^{2+} indicator Fura-2, we investigated the temporal changes in cytosolic Ca^{2+} concentration in three cell models of AS aggregation-dependent cytotoxicity, the mitotic oligodendrocytic cell model OLN-t40-AS, the non-mitotic retinoic acid-differentiated neuroblastoma SH-SY5Y model with inducible AS expression and primary hippocampal neuron cultures from mThy1-αSyn ("line 61") mice (ASO) overexpressing human AS (Fig 1) [13–15]. The OLN-t40-AS model revealed a surprising reduction in cytosolic Ca^{2+} from approximately 195 to 180 nM when measured 8 h after inducing AS aggregation by co-expression of the aggregation-inducing protein p25α (Fig 1A). At this early time point, no overt morphological changes are observed, but early AS aggregation-dependent gene expression responses have been detected like increases in the NF-κB inhibitor, IκBiα [10]. Not surprisingly, an increased cytosolic Ca^{2+} level was measured 24 h after induction of AS aggregation, where cells show visible degenerative changes such as perinuclear microtubule retraction and nuclear NF-κB translocation (Fig EV4B) [10,15]. Both the early decrease and later increase in basal intracellular Ca^{2+} concentration were due to AS aggregation as they could be inhibited by the AS aggregation inhibitor ASI-1D (Fig 1A) [16]. Differentiated non-mitotic SH-SY5Y cells with inducible AS expression displayed a reduction of cytosolic Ca^{2+} from 170 to 150 nM after 5 days of AS expression and an increase after 10 days when compared to b-gal-expressing control cells. Aggregate inhibitor ASI-1D rescued both the initial reduction and late increase (Fig 1B). The biphasic AS aggregation-dependent cytosolic Ca^{2+} change also occurs in primary cultures of mouse hippocampal neurons expressing human AS that display a reduction in cytosolic Ca^{2+} from 150 to 125 nM after 5 days of culture compared to non-transgenic controls and an increase from 150 to 175 nM after 14 days with both phases blocked by ASI-1D (Fig 1C). Hence, using different cell models, we demonstrate a surprising link between early stages of intracellular AS aggregation and cytosolic Ca^{2+} reduction. In order to gain more insight to Ca^{2+} dynamics upon accumulation of AS, we measured Ca^{2+} over time in both the SH-SY5Y model (Fig 1D) and primary hippocampal neurons (Fig 1E). We found that the early phase of decreased cytosolic Ca^{2+} in SH-SY5Y cells is significant from day 4 until day 8, whereas the later Ca^{2+} increase is pronounced after day 10. This closely resembles what we see in primary hippocampal neurons where the early phase of reduced Ca^{2+} is significant between day 5 and 8 and the later phase, with increased Ca^{2+}

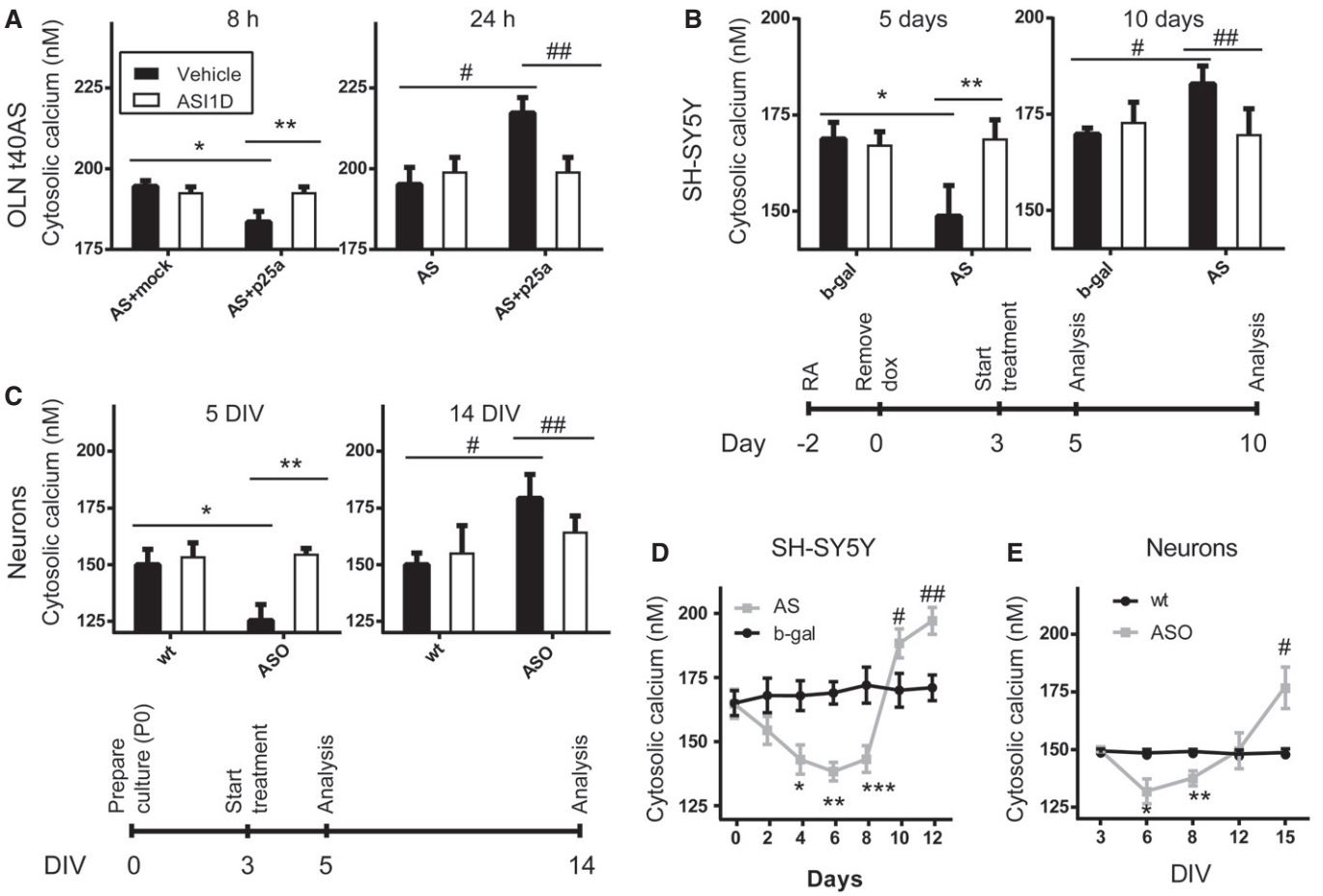

Figure 1. Cellular stress from AS aggregates causes early reduction in cytosolic calcium followed by later increase.
Cytosolic Ca^{2+} levels were quantified by the Ca^{2+} sensor Fura-2 and converted to absolute concentrations using the Fura-2 Calcium Imaging Calibration Kit. The AS aggregation inhibitor ASI-1D (20 μM) was used to validate that phenotypes were aggregate-dependent. Statistical analyses were performed using one-way ANOVA multiple comparisons with Sidak *post hoc* test.

A Mitotic OLN-t40-AS cells were transfected with p25α and the fluorescent transfection marker tdTomato. OLN-t40-AS cells transfected with tdTomato and empty expression vectors served as negative controls. Bars display Ca^{2+} concentrations as mean ± SD, $N = 3$ (*$P = 0.0001$, **$P = 0.0002$, $^{\#}P = 0.0011$, $^{\#\#}P = 0.0033$). The average Ca^{2+} level of individual experiments was calculated by measuring > 50 or more tdTomato expressing cells.

B Non-mitotic SH-SY5Y cells were generated by treatment with retinoic acid (RA; 10 μM) for 2 days, after which AS expression was induced by removal of doxycycline (dox) and cytosolic Ca^{2+} measured after 5 days and 10 days of AS expression. See timeline under bars. Cells induced to express β-galactosidase (b-gal) upon dox removal were used as negative controls. Bars display Ca^{2+} concentrations as mean ± SD, $N = 4$ (*$P = 0.0005$, **$P = 0.0005$, $^{\#}P = 0.0062$, $^{\#\#}P = 0.0055$). The average Ca^{2+} level was calculated by measuring > 200 randomly selected cells in each experiment.

C Primary hippocampal neurons were isolated from new-born (P0) mice expressing human AS under the mThy1 promoter and wild-type (wt) littermates. Cytosolic Ca^{2+} was measured after 5 days *in vitro* (5 DIV) and 14 days *in vitro* culture (14 DIV). See timeline under graphs. Bars display Ca^{2+} concentrations as mean ± SD, $N = 3$ (*$P = 0.002$, **$P = 0.0007$, $^{\#}P = 0.0071$, $^{\#\#}P = 0.0455$). The average cellular Ca^{2+} is based on > 500 neurons per experiment.

D Cytosolic Ca^{2+} in SHSY5Y cells as in (B) measured every second day. Points represent Ca^{2+} concentrations as mean ± SD, $N = 3$ (*$P = 0.0377$, **$P = 0.0057$, ***$P = 0.03$, $^{\#}P = 0.045$, $^{\#\#}P = 0.0229$).

E Cytosolic Ca^{2+} in primary hippocampal neurons as in (C) measured every third day. Points represent Ca^{2+} concentrations as mean ± SD, $N = 3$ (*$P = 0.01$, **$P = 0.0073$, $^{\#}P = 0.0058$).

occurring after day 12 and being significant at day 15 (Fig 1C and E). The OLN-T40-AS cells, the SH-SY5Y AS cells and primary neurons isolated from AS-transgenic mice are based on over-expression of AS but their protein levels of AS are not many fold higher than in total brain lysate from C57BL/6J wt mice (Fig EV1). In the OLN model, the AS level is double as high as in brain homogenate and in the SH-SY5Y model levels after 5 and 10 days of AS expression are approx. 75 and 150% of total brain homogenate, respectively. Primary neurons from wt mice have approx. 50% of the AS in adult mice brain whereas primary neurons from AS-transgenic mice has approx. 80 and 95% at DIV 5 and DIV 14, respectively.

Toxic AS oligomers associate with ER of presymptomatic AS-transgenic mice and in brain fractions from PD brain tissue enriched in ER [17]. The free Ca^{2+} concentration in the ER is approximately 0.5 mM, compared to a concentration of 100 nM in cytosol [18]. This steep gradient is maintained by the high-capacity transmembrane P-type Ca^{2+} ATPase SERCA and is critical for cellular signalling, for example by inositol-1,4,5 tris-phosphate-activated ER

channels. Lowering cytosolic Ca^{2+} requires an active process whereby Ca^{2+} is removed from the cytosol against steep gradients. We hypothesised that the decreased cytosolic Ca^{2+} was caused by AS oligomers activating SERCA. To explore this hypothesis, we first conducted a co-immunoprecipitation experiment to test whether toxic AS oligomers could bind SERCA. The AS oligomers used as bait were purified by gel filtration [19,20] and share aggregate-specific epitopes with AS species in pathological human and mouse brain tissue and insoluble AS filaments [16,17,21]. Freshly eluted from the gel filtration column, the oligomers reveal heterogeneous morphologies in negative stain transmission electron microscopy. Here, an underlying structure of ribbons with a width of 13 nm form spirals with a diameter of around 20 nm which further displayed a tendency to form closed and open circular structures with a diameter of around 40 nm (Fig 2A). As sources for SERCA we used detergent extracts of (i) SERCA2b-rich membrane fractions from mice brains of C57BL/6 OlaHsd (ASdel) mice, which do not express AS, to avoid interference from endogenous mouse AS (Fig 2B), and (ii) SERCA1a-rich rabbit muscle microsomes (Fig EV2A). The extracts were supplemented with purified recombinant human monomeric and oligomeric AS (or PBS as negative control) followed by co-immunoprecipitation using anti-AS IgG conjugated to Sepharose beads. SERCA displayed preferential binding to oligomeric AS with negligible binding to monomeric AS irrespective of its source being muscle or brain (Figs 2B and EV2A). During the pumping cycle, SERCA exhibits two grossly different conformations, namely a Ca^{2+}-bound E1 state and a low Ca^{2+}-affinity E2 state. Using 5 μM Ca^{2+} or 1 μM of the SERCA inhibitor, thapsigargin, it was possible to capture SERCA in the E1 and E2 conformations, respectively [22]. Co-immunoprecipitation of the conformation-trapped SERCA, and AS revealed that AS oligomers bind preferentially to the Ca^{2+}-bound E1 conformation, although binding to E2 is not completely abolished (Fig 2C and D). The higher binding to the Ca^{2+}-bound E1 state is unlikely to be due to Ca^{2+} interactions with AS because this binding is of low affinity with a K_d around 0.5 mM [23]. This indicates that AS oligomer interaction with SERCA displays a high degree of structural specificity as physiological changes in the SERCA structure are able to modulate the binding strength.

To test whether SERCA and AS aggregates also interact in a cell model of AS aggregation-dependent degeneration, we investigated the SH-SY5Y model with proximity ligation assay using an antibody pair of rabbit anti-SERCA and mouse anti-AS (Syn211). The cells were analysed after 5 days of AS expression where they exhibit reduced cytosolic Ca^{2+} (Fig 1B). Proximity ligation assay (PLA)

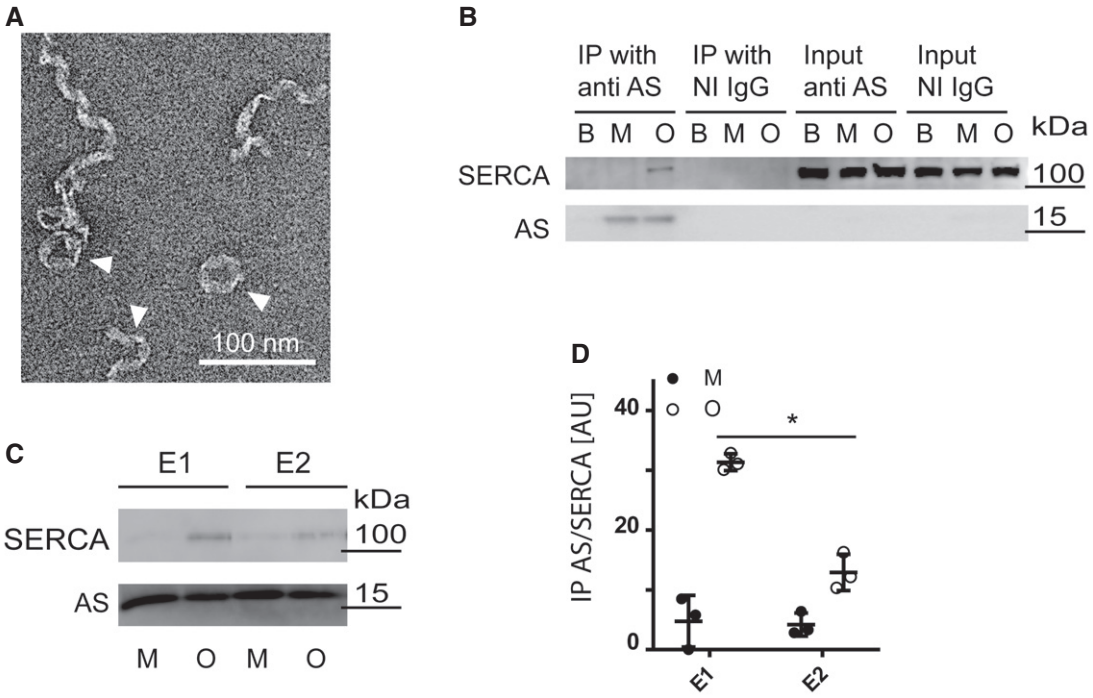

Figure 2. The endoplasmic reticulum calcium ATPase, SERCA, is an AS oligomer-interacting protein.

A Transmission electron microscopy of freshly isolated oligomers. Arrowheads appoint heterogeneous population of twisted ribbons with a maximum width of 15 nm. 100 nm scale bar is presented.

B Purified AS oligomers (O) and monomers (M) were incubated with detergent extract of ASdel mouse brain before being subjected to co-immunoprecipitation (IP) using ASY-1 (anti-AS) and non-immune rabbit IgG (NI IgG) coupled to sepharose. PBS was used as additional negative control. 2% input of each sample was used as input control. The co-IP samples were analysed by immunoblotting anti-SERCA (J15.5) and rabbit polyclonal anti-AS (ASY-1). One representative immunoblot of three independent experiments is shown.

C The Ca^{2+}-bound E1-state of SERCA was stabilised by 5 μM free Ca^{2+}, and the Ca^{2+}-free E2-state was stabilised by 1 μM thapsigargin. A representative blot of three replicates is shown.

D Quantification of immunoprecipitation experiments in (C). Bars represent geometric mean ± 95% CI of SERCA signal relative to the AS signal. $N = 3$ (Wilcoxon signed rank test, $^*P = 0.0382$).

takes advantage of specific secondary antibodies tagged with short, unique DNA strands, termed PLA probes. When complementary PLA probes bind to primary antibodies that are in close proximity (< 40 nm), the DNA strands anneal, allowing enzymatic ligation and amplification of the signal. Fluorescent complementary oligonucleotide probes then label the amplified DNA sequences. AS-SERCA PLA of SH-SY5Y cells that have expressed AS for 5 days reveals that AS is in close proximity with SERCA, as shown by the amplified red punctate signals (Fig 3A). Inhibiting the formation of AS aggregates by ASI-1D treatment completely abolishes the interaction of AS and SERCA (Fig 3B and D), which corroborates the immunoprecipitation data in Fig 2B of only aggregated AS interacting with SERCA. We used a competitive ELISA to validate that ASI-1D does not bind the primary anti-AS antibody Syn211 and thereby artefactually quenches the PLA signal (Fig EV2B). To further validate the specificity of the PLA signal, we suppressed AS expression by doxycycline treatment of transgenic SH-SY5Y cells, and this abolished any PLA signal (Fig 3C and D).

Having demonstrated that AS aggregates can bind SERCA *in vitro* and shown that the interaction occurs in AS aggregate-stressed cells, we wanted to test whether AS oligomers can, indeed, activate SERCA and thus cause reduction in cytosolic Ca^{2+} as observed in AS aggregate-containing cells. First, we investigated the impact on the enzymatic ATPase activity of SERCA. This measurement revealed a dose-dependent increase in ATP hydrolysis by SERCA-containing microsomes when incubated with oligomeric AS in contrast to monomers (Fig 4A). The activation was not due to an inherent ATPase activity in AS oligomers as no hydrolysis was

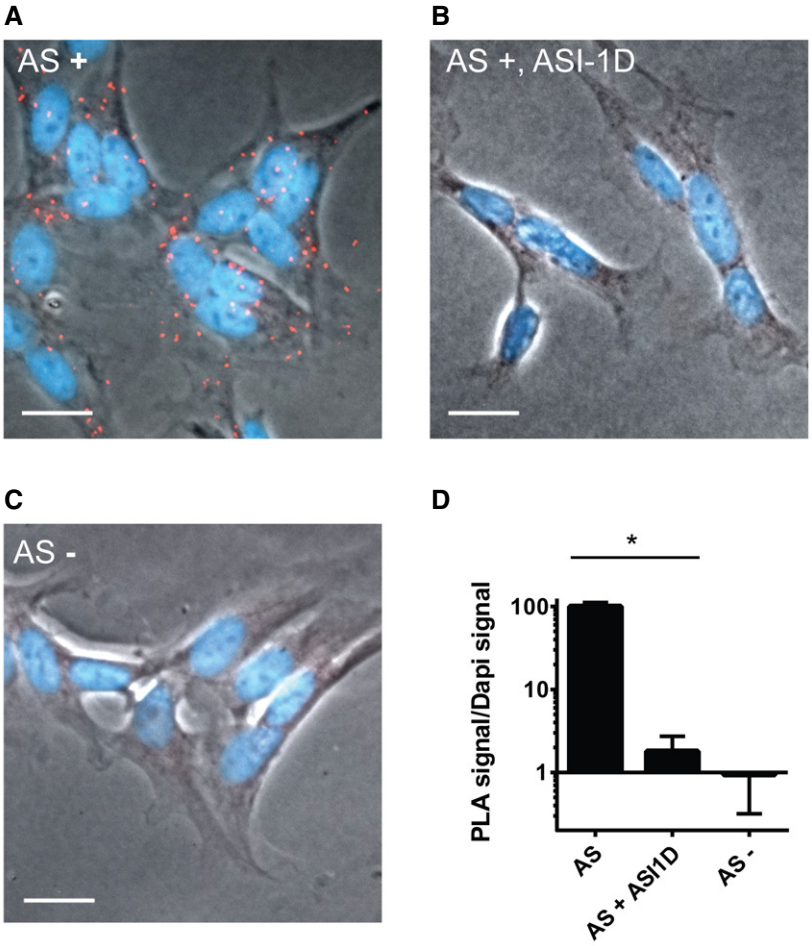

Figure 3. AS aggregates interact with SERCA in SH-SY5Y cells.
Non-mitotic SH-SY5Y cells were grown as depicted in Fig 1B for 5 days after which they were fixed and subjected to proximity ligation assay using Syn211 to target AS and anti-SERCA2. Representative images are from one experiment of three.

A AS-expressing SH-SY5Y cells were analysed by proximity ligation assay to demonstrate an intracellular interaction between SERCA and AS using SERCA2 and syn211 as antibody pair. Positive PLA signals are shown as red staining merged with the phase contrast image and DAPI-stained nuclei (blue). Scale bar is 20 μm.

B Proximity ligation assays as in (A), but with cells treated with AS aggregation inhibitor, ASI-1d, from day 3. Scale bar is 20 μm.

C Proximity ligation assay as in (B), but in cells without AS expression. Scale bar is 20 μm.

D The signal from proximity ligation assay was quantification as total red fluorescence signal, divided by the DAPI signal to normalise cellular content. In each experiment, 10 microscopic images containing > 100 cells were quantified. Bars represent mean ± SD signal normalised to AS-expressing cells from three experiments (one-way ANOVA multiple comparisons with Sidak *post hoc* test, *P = 0.0001).

Published online: March 29, 2018
EMBO reports

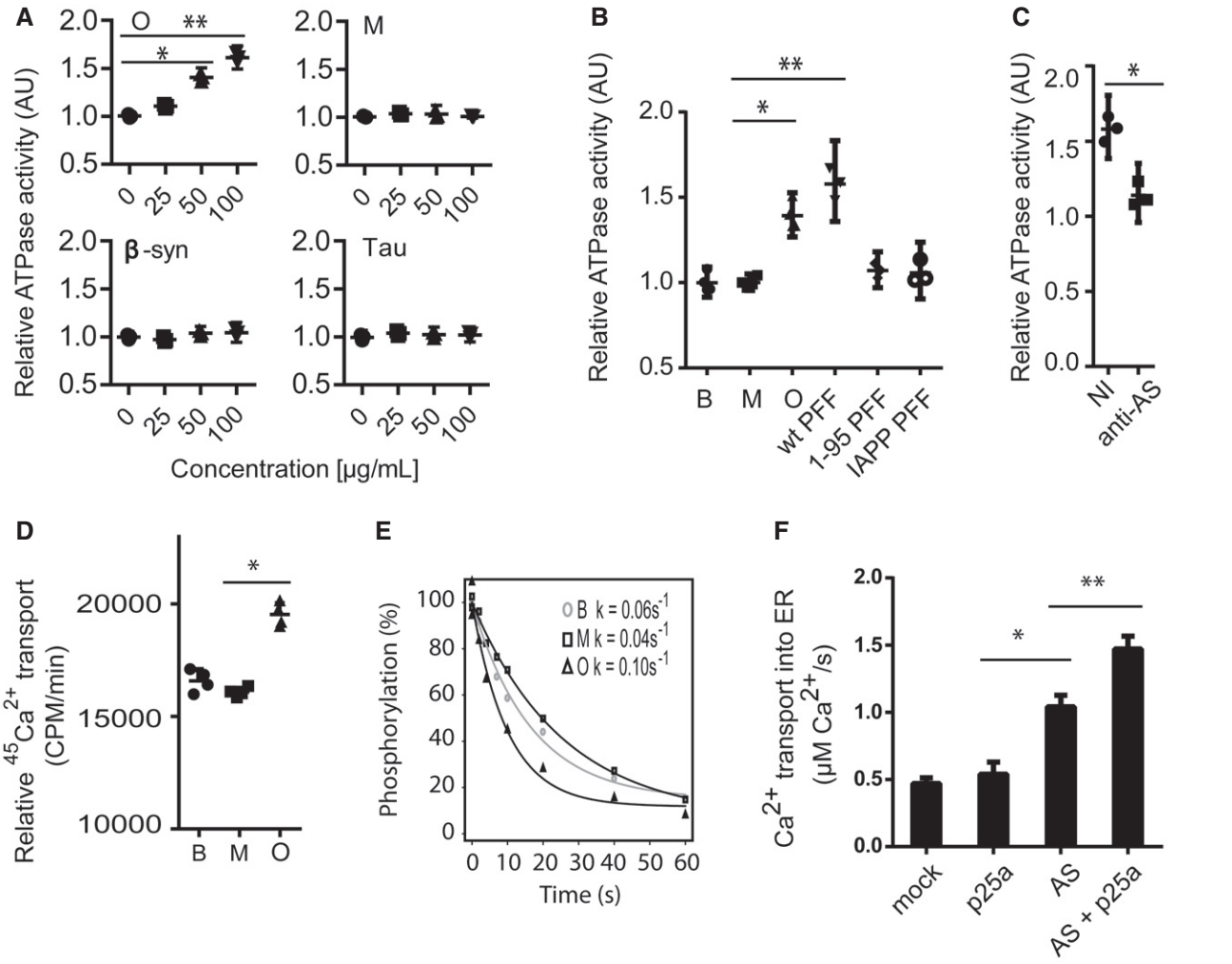

Figure 4. AS oligomers activate SERCA's ATPase activity, calcium pumping and rate of dephosphorylation.

A ATPase activity of SERCA was measured as release of inorganic phosphate from ATP. Sarcoplasmic reticulum (SR) vesicles isolated from rabbit skeletal muscle containing SERCA1a were mixed with AS oligomer (O), AS monomer (M), β-synuclein (β-syn) or Tau in the presence of ATP (5 mM), Ca^{2+} (10 μM) and membrane-permeating ionomycin (2 μM). The ordinate presents ATP hydrolysis within the first 5 min normalised to buffer controls (0 μg/ml). The abscissa presents the concentration of tested proteins. Bars represent the geometric mean of the relative ATP hydrolysis from three individual experiments ± 95% CI (Wilcoxon signed rank test, **P* = 0.0482, ***P* = 0.0034).

B ATPase activity of SERCA was measured as in (A) compared to buffer control (B), but in presence of 50 μg/ml AS monomer (M), oligomer (O), sonicated insoluble fibrils assembled from full-length 1–140 amino acid wild-type AS (wt PFF), sonicated insoluble fibrils assembled from C-terminally truncated 1–95 amino acid AS (1–95 PFF) or sonicated insoluble fibrils assembled from islet amyloid polypeptide (IAPP PFF) that represent a control amyloid-type protein aggregate. Bars represent geometric mean of three individual experiments ± 95% CI (Kruskal–Wallis one-way rank test with Dunn's *post hoc* test, **P* = 0.0161, ***P* = 0.0016).

C Targeting AS oligomer (50 μg/ml) with rabbit polyclonal ASY-1 (1 mg/ml) blocked their ATPase-stimulating activity on SERCA, whereas non-immune rabbit IgG had no effect. Bars represent the geometric mean of three individual experiments ± 95% CI compared to buffer controls (Wilcoxon signed rank test, **P* = 0.048).

D SERCA-dependent Ca^{2+} transport across rabbit muscle ER membranes was measured by accumulation of $^{45}Ca^{2+}$ in ER vesicles in the presence of 50 μg/ml AS oligomers (O), monomer (M) or buffer control (B). Ordinate represents accumulation of $^{45}Ca^{2+}$ in SR vesicles per min measured as counts per minute (CPM). Columns represent the geometric mean of three individual experiments ± 95% CI (Wilcoxon signed rank test, **P* = 0.011).

E The effect of AS oligomers on dephosphorylation of the SERCA E1 state. ^{32}P pre-phosphorylated SERCA was incubated with 50 μg/ml oligomer (O), 50 μg/ml monomer (M) or buffer control in presence of 10 mM EGTA in order to prevent rephosphorylation of SERCA. The residual ^{32}P-SERCA was quantified over time by phospho-imaging of SERCA isolated by acid SDS–PAGE. Ordinate axis represents percentage remaining ^{32}P phosphorylated SERCA and abscissa represents the time. The dephosphorylation rate constants were determined to be k = 0.06/s ± 0.003 for buffer (B), k = 0.04/s ± 0.003 for monomer (M), and k = 0.10/s ± 0.006 for oligomer (O). N = 9 (Kruskal–Wallis one-way rank test with Dunn's *post hoc* test, B vs. O: P = 0.0038 and M vs. O: P = 0.0002).

F The effect of AS aggregation on Ca^{2+} transport into ER in living cells was studied in OLN-t40-AS transfected with low-affinity ER-targeted luminescent aequorin (erAEQ) and co-expression of p25α to induce aggregation. OLN-93 cells without AS were used as negative control. The transport of Ca^{2+} into ER was studied 48 h post-transfection upon supplementing Ca^{2+}-depleted cells with 0.5 mM extracellular Ca^{2+} by measuring increase in luminescence as ER was refilled with Ca^{2+}. Bars represent the mean transport rate of Ca^{2+} into ER ± SD. N = 15 (one-way ANOVA multiple comparison with Sidak *post hoc* test, **P* = 0.0001, ***P* = 0.0023).

observed when the oligomers were incubated with ATP alone (Fig EV3A). Moreover, phosphate release was due to Ca^{2+}- and ATP-dependent mechanisms, ruling out non-specific ATPases and mobilisation of precipitated phosphate (Fig EV3A). To investigate the specificity further, we demonstrated that β-synuclein (β-syn) and Tau proteins had no effect on the ATPase activity of SERCA (Fig 4A). Insoluble preformed AS filaments (PFF) assembled from wild-type full-length AS (wt PFF) also activated SERCA, and this activity was absent in filaments assembled from C-terminally truncated AS (1–95 PFF; Fig 4B). This suggests that activation relies on folding-specific structures requiring the acidic C-terminus and not the core amyloid-type beta-sheet structure formed by the N-terminal 95 residues. To further exclude that a common amyloid-type core structure contributes to SERCA activation, we tested amyloid fibrils assembled from purified islet amyloid polypeptide (IAPP PFF) and observed no activation (Fig 4B). To validate that the activation was not caused by uncharacterised constituents in the preparations, we pre-incubated AS oligomers with rabbit polyclonal antibody ASY-1 targeting AS, and this treatment blocked stimulation in contrast to negative control non-immune rabbit IgG (Fig 4C). The above functional studies were conducted on SERCA1a from rabbit muscle sarcoplasmic reticulum that represents a specialised form of ER, but AS oligomers could also increase the ATP hydrolysis by cellular ER microsomes from COS cells overexpressing the human SERCA1a (Fig EV3B). Second, we studied the effect of AS oligomers on $^{45}Ca^{2+}$ uptake into SERCA-containing microsomes to determine whether increased ATP hydrolysis is due to increased Ca^{2+} pumping or an uncoupled ATP hydrolysis as reported for thermogenic drugs [24]. AS oligomers, but not monomers, increase $^{45}Ca^{2+}$ uptake compared to the buffer control (Fig 4D).

To exclude that the vesicular $^{45}Ca^{2+}$ uptake was due to oligomers making the membrane permeable to Ca^{2+}, we conducted the following control experiment. First, SERCA1a-containing microsomes from rabbit muscles were loaded with $^{45}Ca^{2+}$ and treated with PBS, AS monomers or oligomers for 5 min before the remaining intraluminal $^{45}Ca^{2+}$ was quantified. Ionomycin-treated microsomes served as positive control (Fig EV3C). No difference in $^{45}Ca^{2+}$ efflux could be demonstrated between PBS and the AS preparation in contrast to ionomycin that caused release of all $^{45}Ca^{2+}$ from the microsomes. This strongly argues against AS oligomers forming Ca^{2+}-permeable pores in the biological membranes used in our uptake assay. The Ca^{2+}-transport cycle of SERCA consists of several intermediary steps where dephosphorylation is rate limiting. We studied the effect of AS oligomers on this step by measuring the rate of breakdown of ^{32}P-labelled SERCA after blocking further phosphorylation with EGTA. We thereby demonstrated that AS oligomers stimulate the rate of dephosphorylation in contrast to monomer and buffer control (Fig 4E). We concluded that AS oligomers increase three functional characteristics of SERCA: ATPase activity, transmembrane Ca^{2+} pumping and dephosphorylation.

To corroborate the finding that intracellular AS aggregates do, indeed, activate ER-resident SERCA, we turned to the AS-expressing OLN-93 model where co-expression with p25α stimulates intracellular AS aggregation [15]. OLN-T40-AS cells that stably express human AS were used with the parental OLN-93 line without any AS expression as negative control. ER Ca^{2+} levels were quantified by the ER-targeted low-affinity Ca^{2+}-sensing protein aequorin (erAEQ) [25]. Cells were transfected with p25α or an empty expression vector for 48 h, after which cellular ER Ca^{2+} content was depleted by incubation with ionomycin in the EGTA-supplemented medium. The SERCA-mediated Ca^{2+} uptake rate into the Ca^{2+}-depleted ER was determined by measuring the increase in Ca^{2+}-dependent aequorin luminescence after supplementing the medium with 0.5 mM Ca^{2+} (Fig 4F). The presence of p25α-induced AS aggregates significantly increased the rate of ER filling compared to cells only expressing AS. P25α expression alone did not increase uptake in ER, but OLN-T40-AS cells displayed a greater uptake than the parental OLN-93 cells. It is unclear whether this is due to clonal variation or small amounts of spontaneously forming oligomers. However, induction of AS aggregation in the OLN-t40-AS line by p25α significantly increases ER Ca^{2+} uptake, supporting our hypothesis of intracellular activation of SERCA by AS oligomers. To corroborate the link between SERCA activation and the biphasic cytosolic calcium response, we treated non-mitotic wt SH-SY5Y cells with 10 μM of the SERCA activator XCT 790 [26] in order to mimic the AS aggregate-dependent stimulation. Figure EV4A demonstrates XCT 790 caused an early reduction in cytosolic Ca^{2+} after 4 h followed by a persistent increase in cytosolic Ca^{2+} after 24. This biphasic response is accelerated compared to the AS aggregate-dependent response (Fig 1B) indicating XCT 790 in this concentration is a more potent SERCA activator than aggregated AS.

Taken together, the biochemical demonstration of AS oligomers stimulating SERCA suggests that early reduction in cytosolic Ca^{2+} during AS-dependent degeneration is caused by SERCA stimulation. We further hypothesise that early Ca^{2+} reduction represents a decisive signalling point in the degenerative process. To test this hypothesis in cells, we used the reversible SERCA inhibitor CPA [27–30]. At concentrations around 6 μM, CPA induces mild ER stress with enhanced levels of apoptosis [31], and upon titration, we identified the 10-fold lower 0.5 μM CPA as the minimum concentration that could normalise the reduced Ca^{2+} level in non-mitotic SH-SY5Y cells after AS expression for 5 days. This concentration did not affect the Ca^{2+} levels in the b-gal-expressing control cells (Fig 5A). The cells were treated with CPA from day 3 after transgene expression had been induced by removal of doxycycline as described for ASI-1D treatment in Fig 1B. Surprisingly, CPA treatment by antagonising SERCA-dependent removal of Ca^{2+} from cytosol normalised the abnormally increased cytosolic Ca^{2+} level in the SH-SY5Y after 10 days of transgene expression without any detrimental effects on Ca^{2+} in the controls cells (Fig 5A). Normalising cytosolic Ca^{2+} levels by CPA treatment was beneficial because this treatment significantly reduced AS-dependent cell loss when compared to the b-gal expressing control cells that were unaffected by the treatment (Fig 5B). Normalising cytosolic calcium by CPA treatment also reduced the cell stress in the OLN-T40-AS model after 24 h expression of aggregation-inducing p25α as evidenced by an approximately 50% reduction in nuclear translocation of NF-κB) that compares to the total reduction by treatment with the aggregation inhibitor ASI-1D (Fig EV4B). The biphasic cytosolic Ca^{2+} response in primary hippocampal neurons from AS-transgenic mice was also normalised by CPA treatment from day 3 without affecting Ca^{2+} levels in cultures from wt littermates (Fig 5C). To evaluate the protective effect of CPA treatment on the neuron cultures, we developed a survival assay based on comparing neuron numbers after 6 and 14 days of culture (Fig 5D). Because primary cultures also

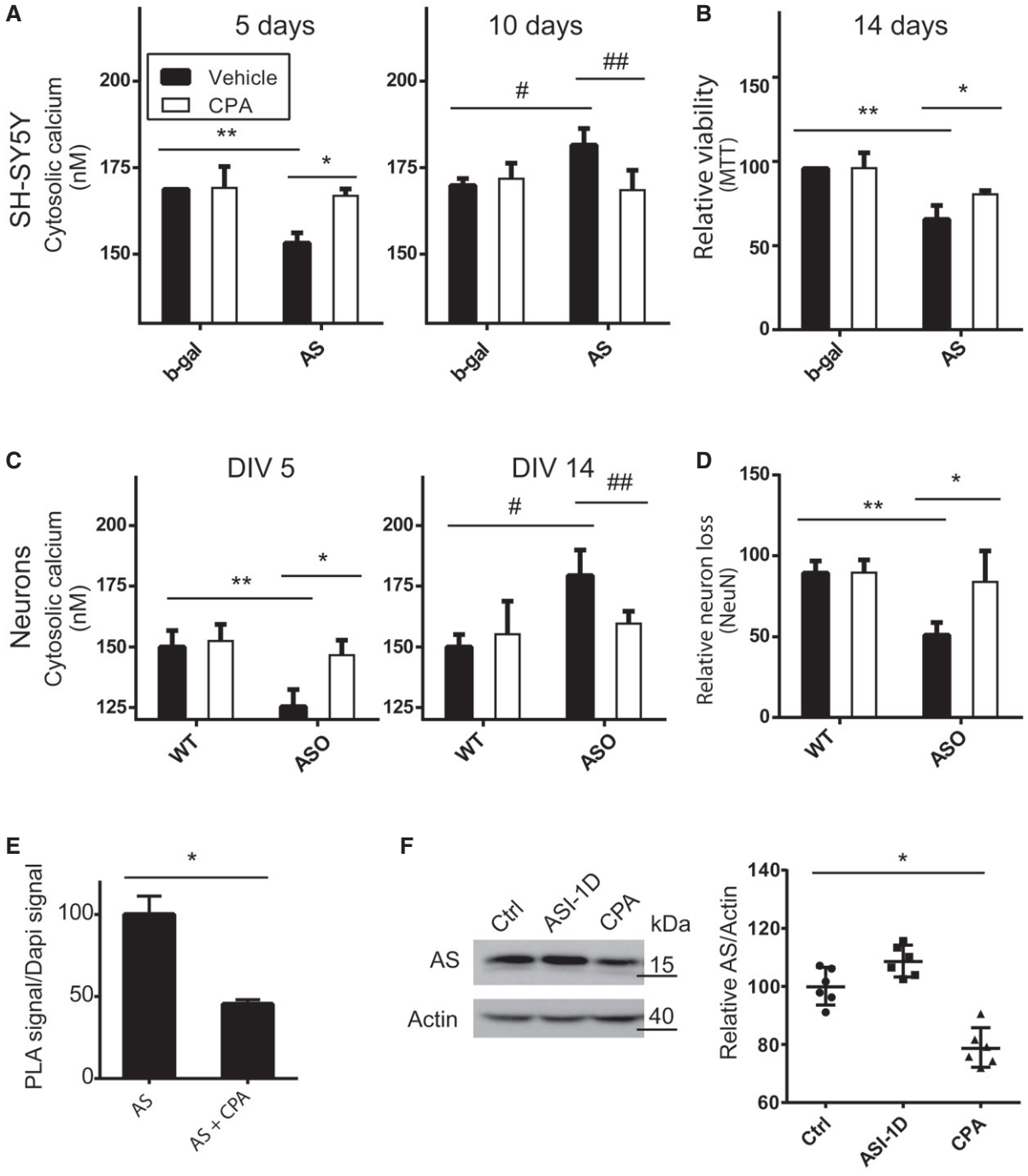

Figure 5.

contain glial cells we used immunostaining of NeuN and MAP2 as neuronal markers (Figs 5D and EV4C). During the period from 6 to 14 days of culture, we saw no significant reduction in non-transgenic primary hippocampal neurons, which contrasts with the approximately 40% loss measured by NeuN and 30% measured by MAP2 in the AS-expressing cultures (Figs 5D and EV4C). The CPA treatment completely protected against AS-induced neuron loss and had no adverse effects on the cultures of non-transgenic littermates (Fig 5D). Treatment with 0.5 μM CPA reduced the interaction between AS and SERCA by approx. 50% (Fig 5E) and reduced total AS levels with 10% (Fig 5F) suggesting the reduced Ca^{2+} level may compromise proteostatic mechanisms.

To test whether SERCA inhibition also is neuroprotective *in vivo,* we took advantage of a *C. elegans* model overexpressing both AS and GFP in dopaminergic neurons under the *dat-1* promoter (*Pdat-1::GFP/AS*). This model displays an AS-dependent degeneration of anterior deirid (ADE) and cephalic (CEP) neurons compared to *C. elegans* which expresses only GFP (*Pdat-1::GFP*) [32–34].

Figure 5. Inhibition of SERCA by cyclopiazonic acid normalises both the early decrease and late increase in cytosolic calcium and enhances the viability in differentiated SH-SY5Y cells and primary neurons.
Cytosolic Ca^{2+} was measured by Fura-2 as described in Fig 1.

A Non-mitotic SH-SY5Y cells were treated with 0.5 μM CPA beginning after 3 days of AS/b-gal expression started using DMSO as solvent control. Bars display Ca^{2+} concentrations as mean ± SD, $N = 3$ (one-way ANOVA multiple comparisons with Sidak *post hoc* test, $^{*}P = 0.014$, $^{**}P = 0.0031$, $^{\#}P = 0.0254$, $^{\#\#}P = 0.0145$). The average Ca^{2+} level was calculated by measuring > 200 randomly selected cells in each experiment.

B Viability of the SHSY5Y cells was measured by the MTT assay for mitochondrial oxidoreductase activity after 14 days of AS or b-gal expression with CPA (0.5 μM) treatment from day 3. Bars represent relative viability normalised to vehicle-treated b-gal cells displayed as mean ± SD. $N = 3$ (one-way ANOVA multiple comparisons with Sidak *post hoc* test, $^{*}P = 0.0002$, $^{**}P = 0.0304$).

C Primary hippocampal neurons from P0 mice expressing human AS (ASO) under the mThy1 promoter and wild-type (wt) littermates were treated with 0.5 μM CPA from day 3 *in vitro* (DIV 3). Cytosolic Ca^{2+} was measured at DIV 5 and DIV 14. Bars represent Ca^{2+} concentrations as mean ± SD, $N = 3$ (one-way ANOVA multiple comparisons with Sidak *post hoc* test, $^{*}P = 0.0041$, $^{**}P = 0.0095$, $^{\#}P = 0.0081$, $^{\#\#}P = 0.0461$). The average Ca^{2+} level was calculated by measuring > 500 randomly selected neurons in each experiment.

D Survival of neurons from day 6 to day 14 was quantified by counting NeuN-positive nuclei. Bars represent remaining Neu^{+} neurons at day 14 normalised to the number present at day 6, presented as means ± SD of four individual experiments with > 400 neurons (one-way ANOVA multiple comparisons with Sidak *post hoc* test, $^{*}P = 0.0033$, $^{**}P = 0.0137$).

E To test the effect of CPA treatment on the interaction between SERCA and AS aggregates, non-mitotic SH-SY5Y cells expressing AS for 5 days were treated with 0.5 μM CPA during the last 2 days. The cells were subjected to AS-SERCA PLA using SERCA2 and syn211 as antibody pair as described in Fig 3. The total red fluorescence signal from the PLA was divided by the DAPI signal to normalise for cellular content. In each experiment, 10 microscopic images containing > 100 cells were quantified. Data are presented as normalised to the signal from non-CPA-treated cells. Bars represent mean ± SD signal normalised to AS-expressing cells from three experiments (one-way ANOVA multiple comparisons with Sidak *post hoc* test $^{*}P = 0.0001$).

F α-syn levels in differentiated SH-SY5Y cells expressing α-syn for 5 days, and treated the last 2 days with 20 μM ASI-1D or 0.5 μM CPA, were measured by immunoblotting. Representative immunoblot is presented. Quantification of α-syn normalised to the actin loading control is presented as geometric mean ± 95% CI for six independent experiments (Wilcoxon signed rank test, $^{*}P = 0.0313$).

Dendrites of the 4 dopaminergic CEP neurons project towards the anterior mouth region and are easily quantifiable by fluorescence microscopy of fixed *C. elegans* [32–34]. We scored absent, discontinuous and beaded dendrites as unhealthy. Examples of healthy and unhealthy *C. elegans* with 4 and 1 intact dendrite are presented in 3D-projected images in Fig 6A. Quantification of healthy CEP dendrites of 8-day-old *C. elegans* is presented in Fig 6B. Control *pdat-1::GFP C. elegans* displayed an age-dependent dendritic loss with an average of 2.1 dendrites remaining. This loss is significantly increased in AS-expressing *pdat1 AS/GFP* worms with only 1.5 dendrites left after 8 days (Fig 6B) representing a 40% larger loss than in control worms. Inhibition of SERCA was initiated on 3-day-old *C. elegans* by transferring them to new bacterial lawns onto which 70 μl 10 mM CPA was evenly distributed. New CPA-covered bacterial lawn was applied at day 6, and worms were fixed at day 8 prior to quantifying their dendrites. CPA treatment of AS-transgenic

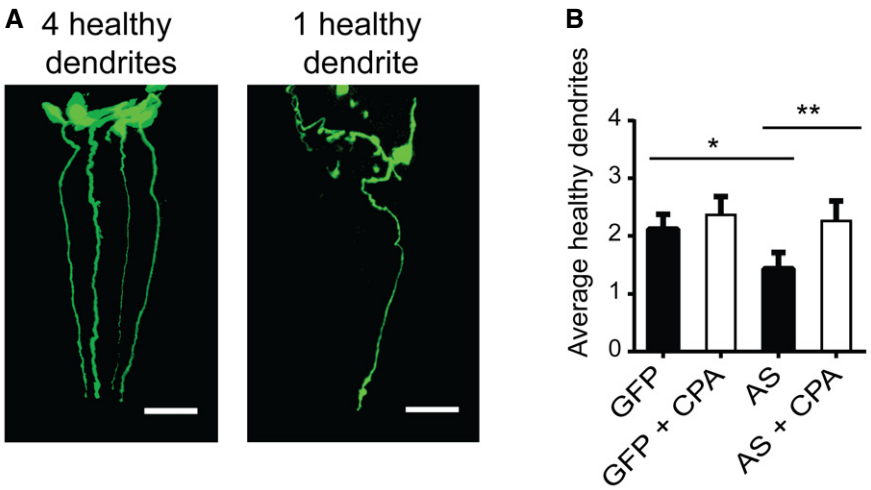

Figure 6. Inhibition of SERCA by cyclopiazonic acid protects against human AS stress-dependent loss of dopaminergic neurons in *C. elegans*.
C. elegans expressing human AS in dopaminergic neurons was used to test the neuroprotective role of SERCA inhibition *in vivo*. *C. elegans* (*Pdat-1::GFP/AS*) overexpressing both human AS and GFP under the *dat-1* promoter was compared to *C. elegans* (*Pdat-1::GFP*) expressing GFP alone, and neurodegeneration was evaluated by quantifying the dendritic projection to the mouth region from the four dopaminergic cephalic (CEP) neurons in the anterior region of *C. elegans*.

A Representation of an 8-day-old *Pdat-1::GFP* worm with four intact CEP neurons determined by the presence of intact anterior projecting dendrites (left) and an 8-day-old *Pdat-1::GFP/AS* worm with one remaining dendrite (right). Images are 3D reconstructions of z-stacks obtained at 63× magnification. Scale bar is 20 μm.

B Quantification of average number of intact CEP neurons per *C. elegans* upon CPA treatment. CPA treatment of *C. elegans* started at day 3. Bars represent the average number of healthy dendrites projecting from CEP neurons ± SD. $N = 4$ (one-way ANOVA multiple comparisons with Sidak *post hoc* test, $^{*}P = 0.0146$, $^{**}P = 0.0008$). > 35 worms per experiment.

worms rescued survival of CEP neurons to the level seen in control worms, but did not affect age-dependent CEP loss in control *C. elegans* (Fig 6B). This indicates that SERCA inhibition by CPA specifically rescues the AS-dependent, but not age-dependent, dendrite loss which supports the hypothesis of SERCA inhibition as a therapeutic strategy in α-synucleinopathies (Fig 8).

To investigate if AS and SERCA interact in human brain, we conducted the AS-SERCA PLA assay on brain sections of occipital cortex from a neurological intact control patient and frontal cortex from a patient affected by DLB (Fig 7A and B). Inspection of images captured from the control patient revealed a low level of PLA-positive signals that always were present as single spots or a few in proximity. By contrast, the DLB patient displayed a large number of labelled cells that often possessed clusters of many PLA signals indicative of larger amounts of complexes in individual cells. This was evident by the significantly increased area covered by PLA signals and also the increased intensity of the signals (Fig 7B). It should be noted that there is a large variation in the amount of PLA signals within DLB tissue suggesting the disease process is heterogeneously affecting the tissue being studied.

The hallmark glial cytoplasmic inclusions (GCI) in MSA presents with insoluble AS fibrils in oligodendroglia. We investigated whether SERCA cosegregates with insoluble AS fibrils in cerebellar extracts from three cases diagnosed with MSA and compared them to three neurological healthy cases (control) where is expected to be detergent soluble. Figure 7C demonstrates the presence of SERCA along with AS in the detergent-insoluble fractions in MSA cases whereas this fraction i in the control cases was devoid of SERCA and AS. This contrasts the total homogenates that displayed similar amounts of SDS-extractable SERCA.

To further investigate the association of SERCA to insoluble AS fibrils in Lewy bodies (LB) and GCI we isolated from the midbrain of a PD patient and glial cytoplasmic inclusions (GCI) from temporal white matter of an MSA patient. We used this purified preparation because they are rich in AS aggregates and devoid of the strong ubiquitous staining that arises from ER present in all brain cells. Immunofluorescence microscopical analysis revealed SERCA epitopes in both midbrain LB and MSA-derived GCI (Fig 7D and F). In LBs, SERCA is present as large granular structures in the core where AS is less abundant, whereas SERCA in GCI displays a more even and less granular presence largely co-localising with AS (Fig 7D and F). We also stained inclusions for the ER protein GRP78 (also known as BiP) to evaluate if the SERCA protein may be embedded in ER when present in the AS-containing inclusion (Fig 7E and G) and could confirm GRP78 is present in both types of inclusions.

Discussion

To the best of our knowledge, we are the first to demonstrate a prolonged cellular state characterised by a reduced level of cytosolic Ca^{2+} in neurons elicited by a progressive build-up of intracellular AS aggregates. The reduced Ca^{2+} level is observed in cell models at an early stage of the degenerative process where cells appear unaffected. Quantitatively, it amounts to an approximately 20% reduction in the resting level in primary hippocampal neurons from 150 to 125 nM. Our observation is corroborated by an X-ray fluorescence study that observed a reduced amount of Ca^{2+} in frozen cultured neurons expressing transgenic human AS, albeit this analysis did not allow for specific assignment of the reduced Ca^{2+} to cytosol [35]. The apparently unaffected or "healthy" phenotype at this early stage may be the reason for the phase staying unrecognised, but another reason is that studies of AS in relation to Ca^{2+} have focussed on dynamic effects like Ca^{2+}-influx induced by depolarisation or effects of applying extracellular AS on stimulation by neurotransmitters [36,37]. The significance of an early degenerative phase was first noted in our OLN cell model [15], where the expression of certain genes was increased early after induction of AS aggregation, which is where we observe decreased cytosolic Ca^{2+} [10]. Silencing one of these genes protected the cells and motivated us to study this phase in more depth [10]. Increases in cytosolic Ca^{2+} can be considered a cellular default response to a range of noxious stimuli that compromises the active and coordinated ion transport processes maintaining the steep gradient of Ca^{2+} ions across membranes. Such increases are hypothesised to represent pathogenic drivers in a range of neurodegenerative states like AD and PD [38,39].

Apart from the study of Ramonet *et al*, where the cation ATPase, ATP13A2 encoded by *PARK9* gene was overexpressed in mouse cortical neurons [40], reduced cytosolic Ca^{2+} for prolonged periods has not been observed in known disease models. However, this can be obtained for limited periods of time by infusion of Ca^{2+} chelators, for example BAPTA, through patch pipettes that elicit acute electrophysiological effects [41,42]. Increased expression of Ca^{2+}-binding proteins has been used to lower Ca^{2+} levels, but this strategy is not optimal for lowering steady-state Ca^{2+} levels. However, it allows changing of Ca^{2+} transients, for example in the study of the effect of glutamate on Ca^{2+}-dependent genes by nuclear targeting of Ca^{2+}-buffering parvalbumin [43]. The reduction of cytosolic Ca^{2+} by intracellular AS aggregates comes at the cost of energy as Ca^{2+} has to be actively transported. Mechanistically, this process can be facilitated by ion exchangers like sodium–Ca^{2+} exchanger (NCX) or by Ca^{2+} pumps. The low basal cytosolic Ca^{2+} level in our models suggests that high-affinity mechanisms are operating in contrast to low affinity but high-capacity NCX transporters. Ca^{2+} pumps are optimal for this process as they have evolved to fine-tune cytosolic Ca^{2+} levels in the nanomolar range [44–46]. We hypothesised that aggregated AS binds directly to and stimulates the predominant Ca^{2+} pumps in the plasma membrane and endoplasmic reticulum, PMCA and SERCA, because total AS levels remain fairly stable in our cell models and the decrease in cytosolic Ca^{2+} is prevented by the aggregation inhibitor ASI-1D. Co-immunoprecipitation experiments followed by proteomic techniques have demonstrated that PMCA from porcine brain binds both monomer and oligomeric AS [20]. Likewise, SERCA was found to bind AS by pull-down experiments; however, pronounced selectivity was seen with strong binding of aggregated AS to SERCA in contrast to very low binding of monomeric AS. The interaction seems to rely on specific structural features of SERCA because the Ca^{2+}-bound E1 state demonstrated stronger interaction with AS than the Ca^{2+}-free thapsigargin-stabilised E2 state. During the E1-E2 transition, the largest structural change in the cytosolic part of SERCA occurs in the actuator domain [47,48], suggesting that this region may be a candidate for binding AS aggregates. The binding of AS oligomers to SERCA resulted in activation of three functional characteristics: Ca^{2+} pumping, ATP

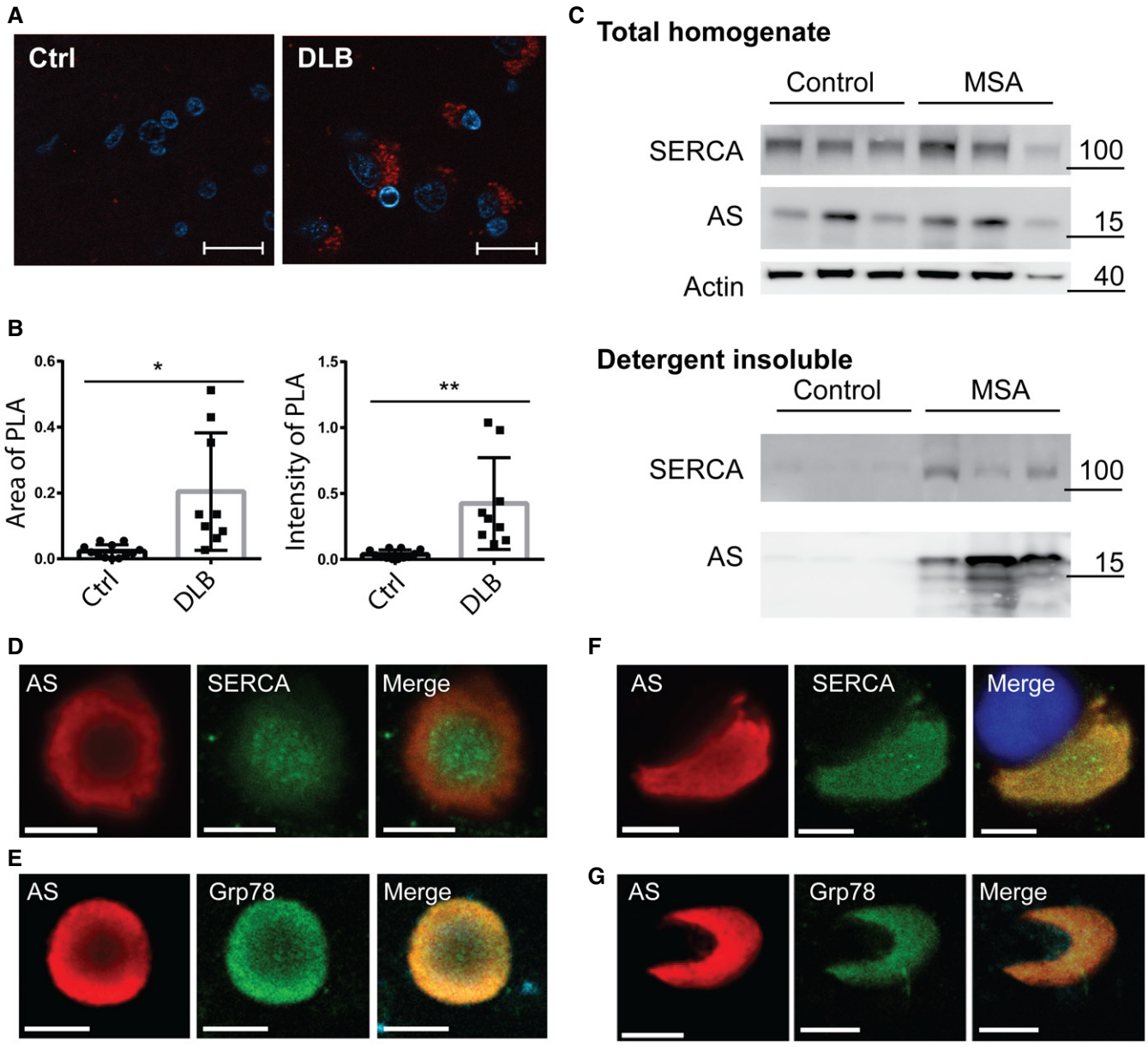

Figure 7. AS and SERCA co-occur in synucleinopathies.

A Representative image of proximity ligation assay using SERCA2 and syn211 as antibody pair on 5-μm sections paraffin-embedded human frontal cortex from DLB case (DLB) and occipital cortex from neurological healthy case (Ctrl). Scale bar is 20 μm.

B The proximity ligation signal was quantified in 10 randomly distributed microscopic images using ImageJ as mean area ± SD covered by PLA signal (left graph) and mean PLA intensity ± SD in the covered area (right graph) of signal above 3× the background signal (Student's *t*-test, **P* = 0.0023, ***P* = 0.0011).

C Immunoblot analysis of extracts from human cerebellar dentate nucleus from three neurological healthy cases (Control) and three cases with multiple system atrophy (MSA). Presented is the total homogenate and the detergent-insoluble fraction solubilised in 5% SDS, 8 M urea prior to immonoblotting analysis (detergent insoluble). The molecular markers for the individual immunoblots are presented to the right of the panels.

D Immunostaining of isolated Lewy body (LB) from a PD patient labelled for AS and SERCA2 immunoreactivity. Scale bar is 5 μm.

E Immunostaining of isolated LB from a patient with DLB labelled for AS and ER marker GRP78. GRP78 reactivity is present in the inclusion. Scale bar is 7.5 μm.

F Immunostaining of isolated glial cytoplasmic inclusion (GCI) from MSA patient labelled for AS and SERCA. DAPI stains a co-isolated oligodendrocyte nucleus. Scale bar is 5 μm.

G Immunostaining of isolated GCI from MSA patient labelled for AS and GRP78. Scale bar is 7.5 μm.

hydrolysis and SERCA dephosphorylation. This suggests that AS aggregates bind to a defined part of SERCA that promotes its overall functionality. In fact, the actuator domain undergoes major structural rearrangements during the E1P-E2P-E2 partial reaction steps involved in dephosphorylation [49], and this reaction sequence is rate limiting for Ca^{2+} pumping and ATP hydrolysis. It is

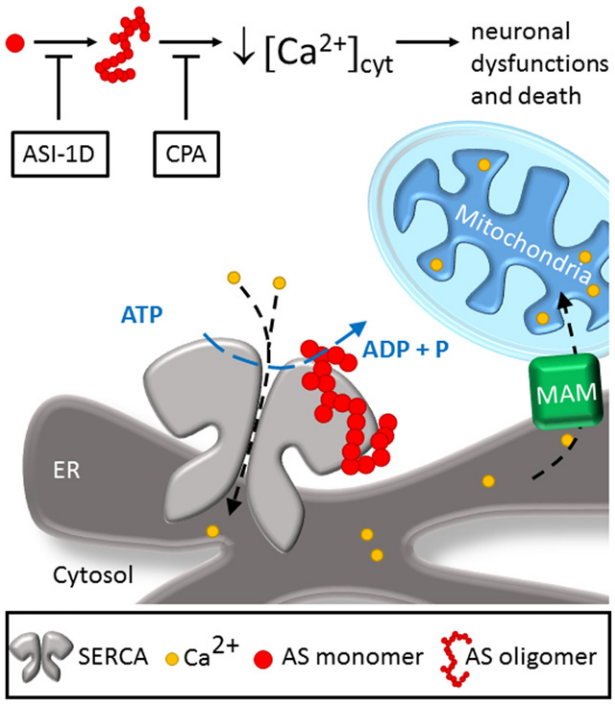

Figure 8. AS aggregates stimulate SERCA activity leading to reduced cytosolic Ca^{2+} and neuron dysfunction and death.
AS aggregates bind and stimulate the active SERCA-mediated transport of cytosolic Ca^{2+} into the endoplasmic reticulum. During the building-up process of cytosolic AS aggregates, the stimulation of SERCA causes an early reduction in cytosolic Ca^{2+}, increased ER Ca^{2+} that could lead to increased mitochondrial Ca^{2+}. The dysregulated Ca^{2+} perturbs Ca^{2+}-dependent processes, leading to progressive neuronal dysfunctions. Ultimately, compensatory mechanisms fail, whereafter cytosolic Ca^{2+} rise and the neurons die. Inhibition of AS aggregation by the inhibitor ASI-1D and reducing the activity of SERCA by its inhibitor CPA counteracts the Ca^{2+} dysregulation and protect the neurons.

thus plausible that interaction of AS aggregates with the actuator domain activates Ca^{2+} pumping and ATP hydrolysis by facilitating the E1P-E2P-E2 steps. The existence of protein-based regulators of SERCA pumps is not unprecedented. Under normal conditions, SERCA activity is inhibited by phospholamban for SERCA1 and -2 [22] and sarcolipin for SERCA1 in skeletal muscle [50]. In contrast, presenilin-1 and -2 have been shown to activate SERCA2b [51], linking SERCA activation to Alzheimer's disease. We studied SERCA1a in most biochemical assays. However, to exclude that the AS oligomer interaction with SERCA studied relies on muscle-specific SERCA properties, we also demonstrated that oligomers stimulate human SERCA1a from microsomes of COS-1 cells overexpressing human SERCA1a and that they bind to SERCA protein in extracts from mouse and porcine brains as determined by immunoprecipitation.

The soluble oligomeric AS aggregates used for binding and functional studies are chemically unmodified [52] in contrast to other *in vitro* produced oligomers that rely on chemical modifications [53,54]. Our oligomers display a folding pattern that differs from insoluble filaments based on HDX-MS investigations [19], but share functional properties with amyloid-type AS filaments like inhibition of 20S proteasomes [21], binding of aggregate-specific antibody FILA-1 [55] and stimulations of SERCA activity (Fig 4B). To visualise the oligomers, we immobilised them on EM grids immediately upon their elution from the gel filtration column. The oligomers displayed an underlying structure of twisted ribbons with a tendency to form closed and open circular structures with a diameter of around 40 nm. These structures resembled the annular structures formed between wild-type and A53T mutant AS that display a diameter in the 50 nm range and with regular height fluctuations [56]. Our oligomer preparation displays greater structural resolution than those previously reported [52,56]. The reason may be our rapid immobilisation on the EM grid, which contrasts with previous studies where samples were stored at 4°C for varying stretches of time before analysis by TEM and analytical ultracentrifugation [52,56]. Low temperatures may adversely affect structural studies of AS oligomers because they dissociate into monomers at 4°C with 15% released after 3 h and 95% after 14 days along with loss of epitopes for conformational-specific antibody FILA-1 [19]; and further cooling to −13°C dissociates even stable amyloid AS fibrils [57]. Our well-characterised oligomer preparation will form a good starting point for generating complexes with purified SERCA for analysis by high-resolution single particle cryo-electron microscopy [58], as such complexes will allow the characterisation of the interphase between the well-characterised SERCA surface and the active surface of the yet uncharacterised AS oligomers. Insoluble fragments of AS filaments may also be used for such studies because they engage SERCA and activate its ATPase activity, but are easier to generate and are more stable than oligomers. AS oligomers have been proposed to function as pores in biological membranes [59–61]. However, most of these reports are based on studies of artificial phospholipid membranes and use high concentrations of oligomers. We recently demonstrated that our AS oligomer preparation is toxic to OLN-93 cells when applied at 70 μg/ml [62]. However, only 15% of the cells died within 24 h, indicating the toxicity was not based on formation of non-specific pores in plasma membranes, but rather caused a stress-triggering toxic response from within the cell, for example by Ca^{2+} entering voltage-gated Ca^{2+} channels [37]. We tested directly if our AS oligomer preparation permeates the microsomes used for the $^{45}Ca^{2+}$ uptake assay at concentrations of 50 μg/ml and found no increased $^{45}Ca^{2+}$ efflux from preloaded microsomes treated with oligomers compared to monomers or buffer (Fig EV3C). We therefore feel confident that the oligomer-stimulated $^{45}Ca^{2+}$ uptake is due to SERCA activation.

The specific SERCA inhibitor CPA can antagonise SERCA activation and was used to investigate the significance of the reduced cytosolic Ca^{2+}. Dose–response experiments demonstrated that chronic treatment with 0.5 μM CPA abrogated the early reduction in cytosolic Ca^{2+} observed in cell models and primary neurons and prevented subsequent Ca^{2+} increase and ensuing AS aggregation-dependent cell death. The effective CPA concentration of 0.5 nM was low compared to what is used to induce unfolded protein stress in cell models [63,64], and it was not toxic to our cell models even after treatment for more than 2 weeks. This was expected because low-dose long-term pharmacological inhibition of SERCA with thapsigargin that causes a sustained increase in cytosolic Ca^{2+} protects against neuronal cell death due to growth factor removal [65]. The prevention of the later phase with increased cytosolic Ca^{2+} is surprising because CPA acts by preventing SERCA pumping Ca^{2+} from cytosol into ER which should thus favour an increase in

cytosolic Ca^{2+}. This suggests that the secondary Ca^{2+} increase represents a breakdown of compensatory processes leading to an unbalanced influx from Ca^{2+} stores, for example enhanced efflux from ER due to sensitisation of ryanodine or inositol-1,4,5 tris-phosphate receptors, Ca^{2+} channels or from extracellular space via dysregulated Ca^{2+} influx channels or exchangers. The protective effect of CPA demonstrates that pivotal degenerative processes are activated during the early phase are amenable to pharmacological intervention. Their nature remains largely unknown but the stress that elicits the cytoprotective NF-κB AS aggregates [10] is reduced in our OLN model upon inhibition of SERCA by CPA (Fig EV4B). NF-κB is increased in PD as determined by accumulation of p65 in midbrain dopaminergic neurons and Lewy body inclusions in PD and DLB [66–70] and it is also activated by disease-causing mutations in LRRK-2 when studied in iPSC-derived neurons [71]. Inhibiting NF-κB signalling in c-REL-deficient mice induces a late onset parkinsonism also comprising accumulation of aggregated AS [72] and the NF-κB inhibitor IκBiα is increased early in anterior cingulate in PD [73] like we demonstrate in our cell model [10]. This suggests protective NF-κB signalling may be of particular importance for the nerve cell populations being vulnerable in PD.

The reduced Ca^{2+} levels do also directly affect the cellular handling of AS as demonstrated by CPA treatment reducing the interaction between AS aggregates and SERCA by PLA assay and lowering levels of total cellular AS suggesting involvement of chaperone and protein catabolic pathways (Fig 5E and F). How this mechanistically is carried out is uncertain. Several investigations have studied direct effects of Ca^{2+} on AS aggregation *in vitro*. They demonstrate a proaggregatory effect of increased Ca^{2+} levels but often with fluorescently labelled AS proteins [74] and those using non-modified proteins used high Ca^{2+} concentrations [23] because the C-terminal Ca^{2+}-binding site in AS has an IC50 around 200 μM) [75]. However, changed Ca^{2+} levels have potential for affecting a range of pathways regulating intracellular AS levels and specific candidates for rescue by CPA treatment are chaperone-mediated autophagy [76], USP-19-dependent excretion of aggregated AS [77] and changed gene expression regulating cytoprotective so-called neuroprotective shield genes that depend on nuclear Ca^{2+} concentration [43]. The neuroprotective effect of CPA against AS aggregate toxicity and thapsigargin against growth factor withdrawal-dependent neuron death [65] demonstrates that SERCA represents a potentially neuroprotective target, but its ubiquitous expression raises concerns regarding adverse effects in other organ systems. However, there is precedence for targeting ubiquitously expressed ion transporting ATPases as exemplified by the cardiotonic steroids targeting Na-K-ATPase, which is used in congestive heart failure with a narrow therapeutic window [78,79]. Importantly, structural studies of the interaction between AS aggregates and SERCA may allow identification of compounds that block this abnormal interaction. In principle, such compounds could target surfaces of the AS aggregate. Although the active surfaces of AS aggregates are unknown, we show that AS requires C-terminal 45 residues in its monomeric building blocks as demonstrated by absent stimulatory activity of filaments formed by C-terminally truncated AS-1-95. This is analogous to what was required to exhibit increased AS aggregate affinity towards p25α protein [21]. This highly negatively charged and proline-rich region of AS has never been resolved in structural studies and the recently described Greek-key type beta-sheet domain resolved in AS filaments terminated around residue 98 [80], so it remains unknown how it contributes to aggregate-dependent functions. Rather than targeting SERCA and AS aggregates, more tractable down-stream targets may be uncovered by studying the degenerative signalling pathways activated during the early low-Ca^{2+} phase, for example protective nuclear NFkB translocation that is attenuated upon CPA treatment (Fig EV4B). Such AS aggregate-dependent dysfunctions may radiate from the endoplasmic reticulum, as this organelle contributes to a multitude of cellular functions including protein sorting, unfolded protein response, excretion of misfolded cytosolic proteins during proteasomal stress, uptake of Ca^{2+} via store-operated Ca^{2+} entry from the plasma membrane and Ca^{2+} loading into mitochondria via mitochondria-associated membranes (MAMS) [81]. The endoplasmic reticulum permeates all neuronal compartments from pre- to post-synaptic structures, and AS aggregates appear to have a preference for targeting endoplasmic reticulum in AS-transgenic mouse and PD brain tissue [17]. The SERCA affinity of oligomers can represent one mechanism whereby they become concentrated at the ER surface, and the activation of its Ca^{2+} transporting activity can affect ER functions including protein folding and Ca^{2+} signalling, for example via ligand-gated ryanodine or inositol-1,4,5 tris-phosphate Ca^{2+} channels. We demonstrate the SERCA activator XCT 790 qualitatively can mimic the AS aggregate effect by first causing a reduction in cytosolic Ca^{2+} that subsequently is followed by an increased Ca^{2+} level that likely reflects a breakdown of compensatory mechanisms (Fig EV4A). Although the biphasic process caused by 10 μM XCT 790 is accelerated, does it suggest that studies of cellular responses to SERCA activators may be used to disentangle the complex response induced by intracellular AS aggregates and which may arise from several AS aggregate-induced dysfunctions, for example caused by low Ca^{2+} stress, ER overload stress, mitochondrial stress and dysfunctional autophagy.

The duration of the period where a neuron encounters reduced average cytosolic Ca^{2+} will likely influence its contribution to the symptomatology of synucleinopathies where the effect of neuronal dysfunction on circuitries may differ from a frank loss of the cell. In the non-mitotic SH-SY5Y model, cells exhibit progressive degeneration where approximately 30% of the cells are lost after 14 days in accordance with previous reports [13]. These cells experienced reduced Ca^{2+} for 6 days of the 2 weeks period, which is a significant part of these non-mitotic cells' life span. According to the Braak hypothesis of prion-like spreading of misfolded AS cytopathology, individual neurons likely encounter a gradual build-up of pathogenic AS species that may last for years before the cells ultimately die. In this process, they may have passed on prion-like AS species to connected neurons and contributed to symptomatology by changing circuitry properties that are modulated by low cytosolic Ca^{2+}. The hypothesis of prion-like spreading of AS cytopathology in the nervous system posits that small amounts of misfolded AS seeds are released from donor cells and taken up in recipient cells. Here, they start a process of templated aggregation of the native AS that would result in a gradual build-up of intracellular aggregates that may span from early oligomeric species to mature amyloid-type fibrils. The time-course for this build-up is unknown, but it can be obtained in transgenic mouse models by inoculation of preformed fibrils or brain extracts from diseased animals, which initiate a neurodegenerative process that traverse several neurons within months [82]. In humans, the process is expected to be much slower. In relation to

the Braak staging of PD, RBD is hypothesised as representing early manifestation with LB development in brainstem regions preceding the spread to midbrain dopaminergic neurons where actual parkinsonism evolve [83]. More than 70% of RBD patients develop PD within 7 years, which suggests that migration of symptom-causing misfolded AS species from the lower brainstem to the midbrain can take several years. To investigate the hypothesis that AS aggregate-dependent effects on SERCA may occur in brain regions not commonly recognised as affected by Lewy body pathology, we studied the frontal cortex from a DLB patient and occipital cortex from an age-matched control using the AS-SERCA PLA assay. Figure 7A and B demonstrates nearly absent signals in the controls brain suggesting no interactions between SERCA and AS aggregates are taking place. By contrast, the DBL brain exhibits strongly increased signal in terms of area covered with PLA signal and intensity of the signals. This strongly corroborates our hypothesis that interactions between SERCA and AS aggregates develop in tissue from patient affected by synucleinopathies. Our data merely serve as proof of concept, but will justify proper clinical studies of selected brain regions from larger patient cohorts affected by different synucleinopathies. The large microheterogeneity observed in the AS-SERCA PLA signal on the stained tissue section calls for further studies in affected cell types and their relation to putative structural differences and tissue responses like neuroinflammation (Fig 7B). To further substantiate the interaction between aggregated AS species and SERCA, we analysed the extracts from the cerebellar dentate nucleus from three MSA patients and three controls. The tissue was subjected to differential extraction to investigate if the normally detergent-soluble SERCA in the MSA cases will co-fractionate with the detergent-insoluble AS aggregates. Figure 7C demonstrates the presence of detergent-insoluble AS in the MSA cases in contrast to the controls and SERCA cosediment with the insoluble AS aggregates. To further describe the relation between aggregated AS and SERCA within the AS fibrils intracellular inclusions, we isolated Lewy bodies from patients affected by PD and DLB and also GCI from a patient affected by MSA. SERCA was preferentially present in the core of the brainstem-type Lewy bodies from the PD patient whereas it was more diffusely distributed along with the fibrillar AS in the less well organised DLB-type Lewy bodies and the GCI. In the inclusions, SERCA colocalised with the ER marker, Grp78, suggesting ER structures may be trapped in the inclusions, which may contribute to ER dysfunctions.

How may these experimental findings reconcile with first previous epidemiological and genetic data on protective effects against PD by L-type Ca^{2+} channel antagonists [2,3] and second the pathoanatomical data on selective vulnerability of neuronal populations in PD that in substantia nigra pars compacta neurons exhibit large Ca^{2+} driven by L-type Ca^{2+} channels [84,85]? First, it should be kept in mind that both the early phase with reduced cytosolic Ca^{2+} and the following phase with increased Ca^{2+} both are inhibited by inhibiting SERCA with CPA. Hence, treatment strategies targeting the high Ca^{2+} phase may still contribute some cellular relief despite not targeting the underlying mechanism. The largest epidemiological study confirmed a protective effect of ongoing treatment with L-type Ca^{2+} channel antagonists but there was no effect of past use, which made the authors suggest the effect could represent a symptomatic relief rather than a true disease modification [3].

In our proposed paradigm of a biphasic basal Ca^{2+} change in neurons experiencing a build-up of AS aggregates, L-type Ca^{2+} channel antagonists may retard or attenuate the second phase with increased cytosolic Ca^{2+} that is associated with development of cell death. An action on the early phase can also be envisioned if expression of CaV1.3 channels partly is regulated by negative feedback from average cytosolic calcium levels. The increased levels of CaV1.3 antigen and mRNA in cortical tissue with no Lewy body pathology from early PD patients [4,5] could represent a response to soluble AS oligomers activating SERCA and reducing average Ca^{2+} in neurons not exhibiting spontaneous pace making changes in Ca^{2+} as in dopaminergic neurons of substantia nigra pars compacta. The ongoing clinical study of early PD patients treated with L-type Ca channel antagonist isradipine may inform about these issues in the near future (ClinicalTrials.gov Identifier: NCT02168842).

The selective vulnerability of neuronal populations lost in PD has allowed certain characteristics of these neurons to be proposed [84]. Areas affected by Lewy body pathology and substantial neuron loss in PD can be exemplified by substantia nigra pars compacta, locus coeruleus, median raphe nucleus. These neuronal populations display diffuse axonal projections and often possess very large numbers of presynaptic terminals [84]. AS is a protein that normally resides in presynapses in high concentrations and its aggregation process is concentration dependent. This makes presynapses likely to be the first sites to experience the build-up of AS aggregates, as supported by proteinase K blotting experiments on cortical tissue affected by dementia with Lewy bodies [86], that secondarily will activate SERCA, increase ATP consumption and reduce cytosolic calcium levels at these sites. A local aggregatory process in terminals may spread within the terminal field of individual neurons as AS readily disperses between terminals of single neurons in a process affected by neuronal activity [87]. The engagement of SERCA pumps in the large terminal fields of vulnerable neurons will increase ATP consumption putting a stress on their mitochondria and the potentially increase oxidative stress. This process be further complicated because the reduced average cytosolic Ca^{2+} may compromise activity-dependent calcium loading into mitochondria thereby compromising their oxidative phosphorylation [88]. When aggregation increases and AS aggregates are transported from terminals into axons and cell bodies then different mechanisms may come into play caused by the SERCA activation both due to lowered calcium, for example in the nucleus [89] and potentially also ER Ca^{2+} overload if not relieved by overload channels [90]. How these mechanisms driven by a reduced average cytosolic Ca^{2+} interacts with cell type-specific effects in vulnerable substantia nigra dopaminergic neurons will have to be tested? They may affect the Ca^{2+}-induced Ca^{2+}-release from ER facilitated by the oscillating in Ca^{2+} driven by the L-type Ca^{2+} channels and thereby the well-described filling of Ca^{2+} into mitochondria [91]. However, the recently described ER overload channel TMCO1 may well add another layer of complexity in conditions where SERCA activation will cause Ca^{2+} overload in ER [90]. However, irrespective of vulnerable areas in PD it should be kept in mind that AS aggregate pathology has potential to affects brain cells on a broader scale. This has been demonstrated by the clinical studies of families with triplications in the SNCA gene that express increased levels of normal AS protein as reviewed [92]. These families often presented with parkinsonism caused by degeneration of the vulnerable substantia nigra pars compacta but often displayed

dementia and other non-motor symptoms at the time of diagnosis or shortly after. This was due to widespread accumulation of aggregated AS in neurons but also glial cells.

Conclusively our demonstration of AS aggregates activating SERCA and causing dysregulation of cytosolic Ca^{2+} holds potential for affecting the above-described PD-associated mechanisms apart from yet undescribed neuronal functions that potentially are tractable (Fig 8). The specific nature of such dysfunctions, their signalling pathways and brain regions affected in the different synucleinopathies merits further investigations.

Materials and Methods

Cell culture and assays

OLN-T40-AS cells [93,94] were transfected with pcDNA3.1 zeo(−) plasmid-expressing AS aggregation-promoting protein, p25α and TdTomato as transfection marker, or mock control (empty vector) [10,15,21,95] by either electroporation by AMAXA Nucleofector®II Kit L using pre-set program A-033 (Life Technologies), or FuGENE® 6 Transfection Reagent (Promega) according to the manufacturer's instructions. SH-SY5Y cells with inducible expression of AS and β-galactosidase (b-gal) were kind gifts from Professors Leonidas Stefani and Kostas Vekrellis [13]. Cells were differentiated using 20 μM all-trans retinoic acid (Molecular Probes/Invitrogen) for 2 days prior to expression of AS and b-gal, which were induced by removal of doxycycline. Primary hippocampal neurons were cultured from new-born wt and Thy1-a-Syn Line 61 (ASO [96]) mice (P0) [97]. Male ASO neurons were compared to neurons prepared from wild-type males from same litter. Neurons isolated from male pubs were only used, due to transgene insertion into X-chromosome and to random X-chromosome inactivation in females. Hippocampi were dissected in ice-cold Hank's balanced salt solution, dissociated in 20 U/ml papain in Leibovitz's L15 medium (L15, Gibco) for 20 min at 37°C, washed twice in L15 medium and titurated in plating medium [MEM (Gibco) supplemented with 5 g/l glucose, 0.2 g/l $NaHCO_3$, 0.1 g/l transferrin, 0.25 g/l insulin, 0.3 g/l L-glutamine and 10% foetal bovine calf serum (heat-inactivated)]. Hippocampal neurons were seeded on Matrigel® matrix (Corning ®)-coated coverslips. After 24 h, the medium was changed to growth medium [MEM supplemented with 5 g/l glucose, 0.2 g/l $NaHCO_3$, 0.1 g/l Transferrin, 0.3 g/l L-glutamine, 1× B-27 supplement, 2 μM cytosine arabinoside and 5% foetal bovine calf serum (heat-inactivated)]. Primary neurons were genotyped for transgenic AS and gender using the primers ASO-sense: 5′-GACGGGTGTGACAGCAGTAGCC-3′, ASO-antisense: 5′-GATGATGGCATGCAGCACTGG-3′ and SRY F: 5′-TTG TCTAGAGAGCATGGAGGGCCATGTCAA-3′, SRY R: 5′-CCACTCCT CTGTGACACTTTAGCCCTCCGA-3′. Neurons and cell lines were kept at 37°C under 5% CO_2, and cell lines were tested for mycoplasma every month. Cells and neurons were treated with either 20 μM aggregation inhibitor ASI-1D (> 98% pure H-RGGAVVTGRRRRRR-NH_2 (Schafer-N, Copenhagen, DK), 10 mM stock in 98% ethanol [16]) or 0.5 μM CPA (Sigma-Aldrich, #C1530, 10 mM stock in DMSO).

The viability of SH-SY5Y cells was evaluated by metabolic activity in an MTT assay (Life Technologies). Viability of primary hippocampal neurons was evaluated as the ratio of NeuN-positive immunostained neuronal nuclei between DIV 14 and DIV 6 or ratio of Map-2 immunostained neuronal cell bodies between DIV 14 and DIV 6. Images were obtained using a Zeiss Observer Z1 inverted microscope equipped with ApoTome.2. Neuronal cells were blindly counted in ten randomly distributed fields throughout the coverslip, > 500 neurons on three coverslips were included in each individual experiment (total of > 1,500 neurons).

Absolute cytosolic Ca^{2+} levels in OLN-T40-AS, SH-SY5Y and primary neurons were determined using the Ca^{2+}-sensitive fluorescent indicator Fura-2-AM (Molecular Probes/Invitrogen) and an Olympus Scan^R high-content fluorescence microscope equipped with Fura-2 filters. Cells were loaded with Fura-2 in sterile filtered HEPES-buffered saline (HBS: 20 mM HEPES, 150 mM NaCl, 5 mM KCl, 1 mM $CaCl_2$, 1 mM $MgCl_2$, 10 mM glucose, pH 7.4) containing 2.5 μM Fura-2 AM, 0.04% pluronic acid, F127 for 30 min at 37°C, 5% CO_2. The Fura-2-containing medium was replaced with fresh HBS without Fura-2 and incubated additionally for 30 min. The fluorescence was measured on an Olympus Scan^R high-content microscope using excitation wavelengths at 340 and 380 nm and emission at 510 nm. The ratio of the fluorescence signal at 510 nm upon excitation at 340 nm and excitation at 380 nm (FL_ex_{340}/FL_ex_{380}) gives a relative Ca^{2+} estimate independent of cell morphology. The cytosolic Ca^{2+} levels in single cells were measured by placing a region of interest (ROI) outside the nucleus. The size of the ROI was set to be 8 μm^2. For OLN cells, at least 50 transfected cells were measured in three independent replicates. For the inducible SH-SY5Y cells and primary neurons, more than 300 cells were measured in three independent experiments. The Fura-2 ratios were converted to molar concentration using Fura-2 Calcium Imaging Calibration Kit (Molecular Probes, F6774), generating a standard curve from 0 to 350 nM Ca^{2+}.

Transport of Ca^{2+} into ER in cells was measured using the OLN cell line as described in Ref. [25]. Cells were plated in a six-well plate and after 8 h transfected by lipofectamine with 1.5 μg plasmid encoding low-affinity ER-targeted aequorin (erAEQ) and 2.5 μg of p25α or empty vector. Twenty-four hour post-transfection, cells were washed, collected and replated on a 96-well plate. After an additional 24 h (48 h after transfection), cells were incubated for 1.5 h at 4°C in Krebs Ringer modified buffer (KRB: 125 mM NaCl, 5 mM KCl, 1 mM Na_3PO_4, 1 mM $MgSO_4$, 5.5 mM glucose, 20 mM HEPES, pH 7.4 at 37°C), supplemented with the 5 μM ionomycin (A23187), 600 μM EGTA and 5 μM coelenterazine n (Invitrogen) in order to deplete ER Ca^{2+} and functionally reconstitute erAEQ. Afterwards, cells were extensively washed with KRB supplemented with 2% bovine serum albumin and 1 mM EGTA. Refilling of the empty ER was obtained by placing the cells in KRB supplemented with 100 μM EGTA and $CaCl_2$ to reach the final concentration of 0.5 mM $CaCl_2$, and the generated light was measured in a Perkin-Elmer Envision plate reader equipped with a two-injector unit. At the end of the experiment, a hypotonic, Ca^{2+}-rich, digitonin-containing solution was added to discharge the remaining aequorin pool. Output data were analysed and calibrated with a custom-made macro-enabled Excel workbook. ER Ca^{2+} uptake speed was calculated as the first derivative using the slope excel function and smoothed for three time points.

Immunostaining

Cells were fixed in 4% paraformaldehyde for 30 min at room temperature (RT) followed by a wash in PBS and 10 min

permeabilisation in 0.1% Triton X-100, 50 mM glycine, 3 mM $CaCl_2$, 2 mM $MgCl_2$, pH 7.4. Unspecific binding was blocked by 3% bovine serum albumin in PBS for 1 h followed by incubation with the primary antibody for 1.5 h [anti-AS (1 μg/ml, ASY-1 [15,21]), anti-SERCA (1 μg/ml, Abcam, ab3625), anti-p65 (NF-κB) (2.5 μg/ml, Cell Signaling Technology, (D14E12) #8242)]. Unbound antibodies were removed by washing in PBS followed by incubation with Alexa Fluor-conjugated secondary antibodies (Life Technologies). Unbound secondary antibodies were removed by washing in PBS before mounting in Prolong Antifade Gold Mountant (Life Technologies). For Duolink® PLA, the previously described ICC protocol was followed until washing after incubation with primary antibodies [anti-AS (1 μg/ml, syn211, Abcam, ab80627) and anti-SERCA2 (1 μg/ml, Abcam, ab3625)] and continued according to the manufacturer's instructions with the Duolink® *In Situ* Red Starter Kit Mouse/Rabbit (Duolink®, Sigma-Aldrich). All PLA experiments were stained and evaluated blinded. Human tissue used for PLA was obtained from brain donors recruited with informed consent through a regional brain donor programme with ethics approval from the Human Research Ethics Committees of South Eastern Sydney Local Health District and the Universities of Sydney and New South Wales (Sydney) which complies with the statement of human experimentation issued by the National Health and Medical Research Council of Australia. Immunohistochemical stainings were conducted on isolated LB and GCIs from fresh-frozen brains from patients with DLB/PD and MSA as described [98–100] using anti-SERCA (1 μg/ml, Abcam, ab3625), anti-AS (ASY-1) and anti-GRP78 (BD Transduction Laboratories™, # 610979).

C. elegans strains and culture

All *C. elegans* strains were maintained at 20°C on standard nematode growth medium (NGM) plates spotted with *Escherichia coli* strain OP50 as the food source. The strain UA44 [baInl1; *Pdat-1::AS*, *Pdat-1::GFP*] expressing AS and GFP in the dopaminergic neurons was a kind gift from the Caldwell laboratory [32–34]. The control strain BZ555 [egIs1(*dat-1::GFP*)] that only expresses GFP in the dopaminergic neurons was obtained from the Caenorhabditis Genetics Center. For the CPA treatment, 35-mm NGM plates with a fixed volume of 4 ml media were used. About 70 μl of CPA in DMSO (10 μM) or 70 μl DMSO as control was spotted on top of the OP50. The plates were set aside for 4 h to allow the CPA to disperse before 30–40 three-day-old worms were transferred to the plates. The worms were moved to fresh plates every other day to provide fresh CPA and avoid cross-contamination with progeny. Eight-day-old worms were fixed overnight at RT in 2% paraformaldehyde, washed three times in PBS and mounted in fluorescence-mounting media (Dako, # S302380-2). The worms were assessed for degeneration of the dopaminergic neurons by fluorescence microscopy on a Zeiss Observer Z1 inverted microscope equipped with Apotome.2. Images were obtained using Pln Apo 63×/1.4 Oil DIC II objective as 3D-projected images of 40 z-stage sections, each 0.3 μm thick, giving a total image depth of 12 μm.

Protein preparations

Recombinant human AS was produced as described [101]. AS oligomers were formed by incubation of 10 mg/ml monomeric AS on ice for 30 min, followed by gel filtration separation of oligomers and monomers according to Lashuel *et al* [52]. A phosphor-free elution buffer, TBS (10 mM Tris–HCl, 140 mM KCl), was used for transmission electron microscopy and ATPase activity assay. AS oligomers were concentrated using Amicon Ultra-15, Ultracell-10k filter device (Millipore). The concentration of AS oligomer was determined by bicinchoninic acid (BCA) protein concentration assay (Pierce).

Fresh brain tissue from C57BL/6 OlaHsd (ASdel) mice, which does not express AS, was dounce-homogenised in threefold excess volume extraction buffer [25 mM MES, 5 mM DTT, 2 mM EDTA, 9% sucrose, Complete Mini Protease Inhibitor (Roche)] compared to the weight of tissue and centrifuged 1,700 *g* at 4°C for 15 min to remove debris and nuclei. The resulting supernatant was further centrifuged at 100,000 *g* for 1 h at 4°C, and the pellet was dounce-homogenised in an extraction buffer containing 0.5% Triton X-100. The homogenate was centrifuged 100,000 *g* for 1 h at 4°C and used as brain membrane extract for co-immunoprecipitation. SERCA1a was prepared as sarcoplasmic reticuli (SR) microsomes by deoxycholate extracts from rabbit muscle sarcoplasmic reticuli [102,103]. Samples were stored at −80°C and thawed on ice immediately before the experiment. The SR microsomes were dissolved in PBS, 1% Triton X-100 for 30 min on ice and subsequently centrifuged at 100,000 *g* for 1 h prior to co-immunoprecipitation.

Human tissue was obtained with informed consent and the experiments conformed to the principles set out in the WMA Declaration of Helsinki and the Department of Health and Human Services Belmont Report. Human cerebellum dentate nuclei (~0.05 g) were dissected from frozen brain slices of three cases of MSA and three neurological healthy cases donated from the Brain Bank at Bispebjerg-Frederiksberg University Hospital (University Hospital of Copenhagen, DNK; approved by the Danish Data Protection Agency, j.no. BBH-2010-06, I-suite 00971). The use of the brain tissue was approved by the regional ethical committee of Region Hovedstaden (DNK), journal no. H-16025210. MSA patients were diagnosed according to the current MSA consensus guidelines [104]. Detailed neuropathological post-mortem evaluations were performed on each MSA brain [105]. The normal controls were free of neurological disorders. The tissue was processed according to Dickson *et al* [106] with minor changes. The tissue was homogenised in 20 volumes (weight/volume) PBS^+ pH 7.4, supplemented with complete protease inhibitor mix (Roche) and phosphatase inhibitors (25 mmol/l NaF, 25 mmol/l β-glycerophosphate, 0.1 mmol/l Na-vanadate). Debri was removed from the homogenate by centrifugation at 1,000 *g* for 10 min. The supernatant (S1) was diluted to a final protein concentration of 1 mg/ml. Equal amounts of S1 were centrifuged at 100,000 *g* for 1 h. The resulting pellets were washed twice in PBS^+, extracted in PBS^+ with 1% Triton X-100 with 0.5% deoxycholate and 0.1% SDS and centrifuged at 100,000 *g* for 1 h. The resulting pellet was washed twice with PBS^+ with 1% Triton X-100 with 0.5% deoxycholate and 0.1% SDS, before complete extraction in PBS^+ with 8 M urea and 5% SDS.

Electron microscopy

Fresh EM samples were prepared as previously described [107]. Specimens were applied on previously glow-discharged homemade

carbon-coated copper girds and incubated for 10 s. Subsequently, specimens were stained three times with 1% uranyl formate solution. Raw micrographs were acquired automatically at 42,000 magnification at specimen level using the Leginon system [108] operated on a Tecnai Spirit BioTWIN TEM at 120 kV acceleration voltage and a Tietz 416 CMOS detector.

Co-immunoprecipitation of AS and SERCA

Detergent extract of SR microsomes from rabbit muscle was used as the source for SERCA, and its conformations were stabilised in E1 conformation by 5 μM Ca^{2+} or in E2 conformation by 1 μM thapsigargin (Sigma-Aldrich, # T9033). AS oligomer or monomer (2 μg/ml) was mixed with 0.5 mg/ml ASdel mouse brain detergent extract of membrane fraction, or 4 μg/ml SERCA 1A detergent extract of SR microsomes from rabbit muscle *t* in PBS, 0.5% Triton X-100 and incubated overnight at 4°C. AS binding (ASY-1) or control (non-immune IgG) sepharose beads were added in 5× molar excess compared to AS. The samples were incubated for 2 h with rotation. Sepharose beads were isolated by centrifugation in a tabletop centrifuge at 800 *g* for 1 min and washed twice in PBS, 0.5% Triton X-100. The bound protein was extracted in SDS Laemmli buffer without reducing dithiothreitol for 30 min at 37°C. Extracted immunoprecipitated proteins were separated on 10–16% SDS–PAGE, electroblotted onto PVDF membranes; immunoreactivity to AS was evaluated by anti-AS (ASY-1) and SERCA was evaluated by polyclonal rabbit anti-SERCA (raised against the peptide of amino acid 809-827 [109], a kind gift from Professor J.V. Møller, University of Aarhus, DK).

Functional studies of SERCA

The ATPase activity of SERCA was studied by monitoring the release of inorganic phosphate [110]. Transport Ca^{2+} by SERCA was measured as accumulation of $^{45}Ca^{2+}$ in microsomal vesicles, which were quenched with $LaCl_3$ followed by capture by filtration [111]. Combined assays to simultaneously measure Ca^{2+}-activated ATP hydrolysis and ATP-driven Ca^{2+} uptake were conducted with SR vesicles at 37°C in a medium containing 20 mM MOPS/Tris, pH 6.8, 100 mM KCl, 5 mM $MgCl_3$, 5 mM potassium oxalate, 0.5 mM EGTA and 0.45 mM $CaCl_2$ (free Ca^{2+} approx. 10 μM). The medium used for Ca^{2+}-uptake measurements also contained $^{45}Ca^{2+}$ (approx. 0.1 MBq/ml) to trace Ca^{2+} accumulation in the vesicles. The reaction was initiated by addition of 5 mM ATP. This system was also used to investigate leakage of $^{45}Ca^{2+}$ from preloaded microsomes with the exception of the absence of oxalate. In brief, the microsomes were preloaded with $^{45}Ca^{2+}$ overnight at RT and then incubated at 37°C with AS, buffer or ionomycin for 5 min before quenching by $LaCl_3$ and capturing on filter. Furthermore, dephosphorylation of ^{32}P pre-phosphorylated SERCA was followed by serial time interval quantification of acid-quenched SERCA on SDS–PAGE [102,111]. Pre-phosphorylation of SERCA was conducted at 0°C for 15 s in the presence of 5 μM [γ-^{32}P]ATP and 40 mM MOPS/Tris, pH 7.0, 122 mM KCl, 5 mM $MgCl_2$, 1 mM EGTA and $CaCl_2$ to give a free Ca^{2+} concentration of 10 μM, and terminated by addition of 10 mM EGTA to chelate Ca^{2+}. The rate of dephosphorylation was followed over time by acid-quenching the reaction at serial time intervals, and the phosphoenzyme in the quenched samples was isolated by acidic SDS–PAGE and quantified using the Packard Cyclone™ storage phosphor system [111]. The dephosphorylation rate constants were determined as mono-exponential decay function using the SigmaPlot program (SPSS, Inc.).

Enzyme-linked immunosorbent assay

A 96-well maxisorb plate was coated with Syn211 (1 μg/ml) and incubated for 2 h at RT. The plate was washed with TBS-T and blocked in 10% foetal calf serum for 2 h at RT followed by incubation with 0.7 nM biotinylated AS overnight at 4°C with or without increasing amounts of non-biotinylated AS (3.5, 7 or 35 nM) or ASI-1D (5, 10 or 20 μM). After washing, streptavidin-conjugated HRP was added for 2 h at RT followed by addition of TMB. The reaction was stopped by addition of 1 M phosphoric acid, and absorbance was measured at 450 nm.

Statistical analysis

Statistical evaluation of results was performed using parametric tests for data sets following normal distribution by comparing means ± SD. For smaller data sets where normal distribution could not be proven, statistical evaluation was conducted by nonparametric tests and data presented as geometric mean ± 95% confidence interval. In order to compare one mean to another mean, Student's *t*-test was conducted as parametric test and Wilcoxon signed rank test was used as nonparametric test. In order to test the null-hypothesis in multiple comparisons, when comparing several groups to one mean, one-way ANOVA combined with Sidak *post hoc* test was applied as parametric test and Kruskal–Wallis one-way rank test with Dunn's *post hoc* test was applied as nonparametric test to obtain an adjusted *P*-value using the GraphPad Prism program (GraphPad Software). *P*-values below 0.05 are considered to be statistically significant.

Expanded View for this article is available online.

Acknowledgements
The authors acknowledge the Caldwell laboratory at University of Alabama, USA, for sharing the *C. elegans* model overexpressing AS. The original *C. elegans* strains were provided by the CGC, which is funded by NIH Office of Research Infrastructure Programs (P40 OD010440). In addition, the authors wish to thank Prof. Daniel Otzen at iNano, Aarhus University, Denmark, for generously donating islet amyloid polypeptide and Drs Tie-Shan Tang and Aimin Zhou etc. for valuable discussion on ER Ca^{2+} overload. The authors also acknowledge Dr. Bo Martin Bibby, Department of Biostatistics, Aarhus University for the statistical assistance. The Lundbeckfoundation, Dandrite, Aarhus University, the Michael J. Fox Foundation and Parkinsonforeningen are thanked for generous support.

Author contributions
CB planned, executed and analysed most experiments and wrote the manuscript. LBL, RHK, LR, EG and JZ contributed critically to aspects of the project. W-PG and TCh isolated Lewy bodies and glial cytoplasmic inclusions from human brain material. AM performed negative staining electron microscopy. MB and TCa performed the experiments on alpha-synuclein stimulated Ca^{2+} uptake in ER. GH and YF performed the immunohistochemical analyses on human brain tissue. TB, SA and BP isolated the tissue from frozen MSA and control brains. JPA supervised and assisted in the *in vitro* analysis of SERCA

functions. AO conducted the *C. elegans* experiments. PHJ was part of all planning and supervised analyses and final writing of manuscript.

Conflict of interest

The authors declare that they have no conflict of interest.

References

1. Nussbaum RL (2017) Genetics of synucleinopathies. *Cold Spring Harb Perspect Med* https://doi.org/10.1101/cshperspect.a024109
2. Ritz B, Rhodes SL, Qian L, Schernhammer E, Olsen JH, Friis S (2010) L-type calcium channel blockers and Parkinson disease in Denmark. *Ann Neurol* 67: 600 – 606
3. Pasternak B, Svanstrom H, Nielsen NM, Fugger L, Melbye M, Hviid A (2012) Use of calcium channel blockers and Parkinson's disease. *Am J Epidemiol* 175: 627 – 635
4. Hurley MJ, Brandon B, Gentleman SM, Dexter DT (2013) Parkinson's disease is associated with altered expression of CaV1 channels and calcium-binding proteins. *Brain* 136: 2077 – 2097
5. Hurley MJ, Gentleman SM, Dexter DT (2015) Calcium CaV1 channel subtype mRNA expression in Parkinson's disease examined by *in situ* hybridization. *J Mol Neurosci* 55: 715 – 724
6. Surmeier DJ, Schumacker PT, Guzman JD, Ilijic E, Yang B, Zampese E (2017a) Calcium and Parkinson's disease. *Biochem Biophys Res Commun* 483: 1013 – 1019
7. Lieberman OJ, Choi SJ, Kanter E, Saverchenko A, Frier MD, Fiore GM, Wu M, Kondapalli J, Zampese E, Surmeier DJ *et al* (2017) Alpha-synuclein dependent calcium entry underlies differential sensitivity of cultured SN and VTA dopaminergic neurons to a Parkinsonian neurotoxin. *eNeuro* 4: ENEURO.0167-17.2017
8. Braak H, Del Tredici K, Rub U, de Vos RA, Jansen Steur EN, Braak E (2003) Staging of brain pathology related to sporadic Parkinson's disease. *Neurobiol Aging* 24: 197 – 211
9. Bezprozvanny IB (2010) Calcium signaling and neurodegeneration. *Acta Naturae* 2: 72 – 82
10. Kragh CL, Gysbers AM, Rockenstein E, Murphy K, Halliday GM, Masliah E, Jensen PH (2014) Prodegenerative IkappaBalpha expression in oligodendroglial alpha-synuclein models of multiple system atrophy. *Neurobiol Dis* 63: 171 – 183
11. Hamza TH, Chen H, Hill-Burns EM, Rhodes SL, Montimurro J, Kay DM, Tenesa A, Kusel VI, Sheehan P, Eaaswarkhanth M *et al* (2011) Genome-wide gene-environment study identifies glutamate receptor gene GRIN2A as a Parkinson's disease modifier gene via interaction with coffee. *PLoS Genet* 7: e1002237
12. Yamada-Fowler N, Fredrikson M, Soderkvist P (2014) Caffeine interaction with glutamate receptor gene GRIN2A: Parkinson's disease in Swedish population. *PLoS One* 9: e99294
13. Vekrellis K, Xilouri M, Emmanouilidou E, Stefanis L (2009) Inducible over-expression of wild type alpha-synuclein in human neuronal cells leads to caspase-dependent non-apoptotic death. *J Neurochem* 109: 1348 – 1362
14. Rockenstein E, Mallory M, Hashimoto M, Song D, Shults CW, Lang I, Masliah E (2002) Differential neuropathological alterations in transgenic mice expressing alpha-synuclein from the platelet-derived growth factor and Thy-1 promoters. *J Neurosci Res* 68: 568 – 578
15. Kragh CL, Lund LB, Febbraro F, Hansen HD, Gai WP, El-Agnaf O, Richter-Landsberg C, Jensen PH (2009) Alpha-synuclein aggregation and Ser-129 phosphorylation-dependent cell death in oligodendroglial cells. *J Biol Chem* 284: 10211 – 10222
16. El-Agnaf OM, Paleologou KE, Greer B, Abogrein AM, King JE, Salem SA, Fullwood NJ, Benson FE, Hewitt R, Ford KJ *et al* (2004) A strategy for designing inhibitors of alpha-synuclein aggregation and toxicity as a novel treatment for Parkinson's disease and related disorders. *FASEB J* 18: 1315 – 1317
17. Colla E, Jensen PH, Pletnikova O, Troncoso JC, Glabe C, Lee MK (2012) Accumulation of toxic alpha-synuclein oligomer within endoplasmic reticulum occurs in alpha-synucleinopathy *in vivo*. *J Neurosci* 32: 3301 – 3305
18. Yu R, Hinkle PM (2000) Rapid turnover of calcium in the endoplasmic reticulum during signaling. Studies with cameleon calcium indicators. *J Biol Chem* 275: 23648 – 23653
19. Mysling S, Betzer C, Jensen PH, Jorgensen TJ (2013) Characterizing the dynamics of alpha-synuclein oligomers using hydrogen/deuterium exchange monitored by mass spectrometry. *Biochemistry* 52: 9097 – 9103
20. Betzer C, Movius AJ, Shi M, Gai WP, Zhang J, Jensen PH (2015) Identification of synaptosomal proteins binding to monomeric and oligomeric alpha-synuclein. *PLoS One* 10: e0116473
21. Lindersson E, Beedholm R, Hojrup P, Moos T, Gai W, Hendil KB, Jensen PH (2004) Proteasomal inhibition by alpha-synuclein filaments and oligomers. *J Biol Chem* 279: 12924 – 12934
22. Brini M, Carafoli E (2009) Calcium pumps in health and disease. *Physiol Rev* 89: 1341 – 1378
23. Nielsen MS, Vorum H, Lindersson E, Jensen PH (2001) Ca^{2+} binding to alpha-synuclein regulates ligand binding and oligomerization. *J Biol Chem* 276: 22680 – 22684
24. Mahmmoud YA, Gaster M (2012) Uncoupling of sarcoplasmic reticulum Ca(2)(+)-ATPase by N-arachidonoyl dopamine. Members of the endocannabinoid family as thermogenic drugs. *Br J Pharmacol* 166: 2060 – 2069
25. Cali T, Ottolini D, Negro A, Brini M (2012) alpha-Synuclein controls mitochondrial calcium homeostasis by enhancing endoplasmic reticulum-mitochondria interactions. *J Biol Chem* 287: 17914 – 17929
26. Gruber SJ, Cornea RL, Li J, Peterson KC, Schaaf TM, Gillispie GD, Dahl R, Zsebo KM, Robia SL, Thomas DD (2014) Discovery of enzyme modulators via high-throughput time-resolved FRET in living cells. *J Biomol Screen* 19: 215 – 222
27. Thastrup O, Dawson AP, Scharff O, Foder B, Cullen PJ, Drobak BK, Bjerrum PJ, Christensen SB, Hanley MR (1994) Thapsigargin, a novel molecular probe for studying intracellular calcium release and storage. 1989. *Agents Actions* 43: 187 – 193
28. Seidler NW, Jona I, Vegh M, Martonosi A (1989) Cyclopiazonic acid is a specific inhibitor of the Ca^{2+}-ATPase of sarcoplasmic reticulum. *J Biol Chem* 264: 17816 – 17823
29. Foskett JK, Wong D (1992) Calcium oscillations in parotid acinar cells induced by microsomal Ca(2+)-ATPase inhibition. *Am J Physiol* 262: C656 – C663
30. Takahashi M, Kondou Y, Toyoshima C (2007) Interdomain communication in calcium pump as revealed in the crystal structures with transmembrane inhibitors. *Proc Natl Acad Sci USA* 104: 5800 – 5805
31. Miani M, Barthson J, Colli ML, Brozzi F, Cnop M, Eizirik DL (2013) Endoplasmic reticulum stress sensitizes pancreatic beta cells to interleukin-1beta-induced apoptosis via Bim/A1 imbalance. *Cell Death Dis* 4: e701
32. Cao S, Gelwix CC, Caldwell KA, Caldwell GA (2005) Torsin-mediated protection from cellular stress in the dopaminergic neurons of *Caenorhabditis elegans*. *J Neurosci* 25: 3801 – 3812

33. Tucci ML, Harrington AJ, Caldwell GA, Caldwell KA (2011) Modeling dopamine neuron degeneration in *Caenorhabditis elegans*. *Methods Mol Biol* 793: 129 – 148
34. Dexter PM, Caldwell KA, Caldwell GA (2012) A predictable worm: application of *Caenorhabditis elegans* for mechanistic investigation of movement disorders. *Neurotherapeutics* 9: 393 – 404
35. Ducic T, Carboni E, Lai B, Chen S, Michalke B, Lazaro DF, Outeiro TF, Bahr M, Barski E, Lingor P (2015) Alpha-synuclein regulates neuronal levels of manganese and calcium. *ACS Chem Neurosci* 6: 1769 – 1779
36. Hettiarachchi NT, Parker A, Dallas ML, Pennington K, Hung CC, Pearson HA, Boyle JP, Robinson P, Peers C (2009) alpha-Synuclein modulation of Ca^{2+} signaling in human neuroblastoma (SH-SY5Y) cells. *J Neurochem* 111: 1192 – 1201
37. Melachroinou K, Xilouri M, Emmanouilidou E, Masgrau R, Papazafiri P, Stefanis L, Vekrellis K (2013) Deregulation of calcium homeostasis mediates secreted alpha-synuclein-induced neurotoxicity. *Neurobiol Aging* 34: 2853 – 2865
38. Mattson MP (2007) Calcium and neurodegeneration. *Aging Cell* 6: 337 – 350
39. Bezprozvanny I (2009) Calcium signaling and neurodegenerative diseases. *Trends Mol Med* 15: 89 – 100
40. Ramonet D, Podhajska A, Stafa K, Sonnay S, Trancikova A, Tsika E, Pletnikova O, Troncoso JC, Glauser L, Moore DJ (2012) PARK9-associated ATP13A2 localizes to intracellular acidic vesicles and regulates cation homeostasis and neuronal integrity. *Hum Mol Genet* 21: 1725 – 1743
41. Konnerth A, Dreessen J, Augustine GJ (1992) Brief dendritic calcium signals initiate long-lasting synaptic depression in cerebellar Purkinje cells. *Proc Natl Acad Sci USA* 89: 7051 – 7055
42. Roussel C, Erneux T, Schiffmann SN, Gall D (2006) Modulation of neuronal excitability by intracellular calcium buffering: from spiking to bursting. *Cell Calcium* 39: 455 – 466
43. Mauceri D, Hagenston AM, Schramm K, Weiss U, Bading H (2015) Nuclear calcium buffering capacity shapes neuronal architecture. *J Biol Chem* 290: 23039 – 23049
44. Brini M, Carafoli E, Cali T (2017) The plasma membrane calcium pumps: focus on the role in (neuro)pathology. *Biochem Biophys Res Commun* 483: 1116 – 1124
45. Vandecaetsbeek I, Vangheluwe P, Raeymaekers L, Wuytack F, Vanoevelen J (2011) The Ca^{2+} pumps of the endoplasmic reticulum and Golgi apparatus. *Cold Spring Harb Perspect Biol* 3: a004184
46. Giladi M, Tal I, Khananshvili D (2016) Structural features of ion transport and allosteric regulation in sodium-calcium exchanger (NCX) proteins. *Front Physiol* 7: 30
47. Toyoshima C, Nomura H (2002) Structural changes in the calcium pump accompanying the dissociation of calcium. *Nature* 418: 605 – 611
48. Sorensen TL, Moller JV, Nissen P (2004) Phosphoryl transfer and calcium ion occlusion in the calcium pump. *Science* 304: 1672 – 1675
49. Toyoshima C (2009) How Ca^{2+}-ATPase pumps ions across the sarcoplasmic reticulum membrane. *Biochim Biophys Acta* 1793: 941 – 946
50. Odermatt A, Becker S, Khanna VK, Kurzydlowski K, Leisner E, Pette D, MacLennan DH (1998) Sarcolipin regulates the activity of SERCA1, the fast-twitch skeletal muscle sarcoplasmic reticulum Ca^{2+}-ATPase. *J Biol Chem* 273: 12360 – 12369
51. Green KN, Demuro A, Akbari Y, Hitt BD, Smith IF, Parker I, LaFerla FM (2008) SERCA pump activity is physiologically regulated by presenilin and regulates amyloid beta production. *J Cell Biol* 181: 1107 – 1116
52. Lashuel HA, Petre BM, Wall J, Simon M, Nowak RJ, Walz T, Lansbury PT Jr (2002) Alpha-synuclein, especially the Parkinson's disease-associated mutants, forms pore-like annular and tubular protofibrils. *J Mol Biol* 322: 1089 – 1102
53. Danzer KM, Haasen D, Karow AR, Moussaud S, Habeck M, Giese A, Kretzschmar H, Hengerer B, Kostka M (2007) Different species of alpha-synuclein oligomers induce calcium influx and seeding. *J Neurosci* 27: 9220 – 9232
54. Nasstrom T, Fagerqvist T, Barbu M, Karlsson M, Nikolajeff F, Kasrayan A, Ekberg M, Lannfelt L, Ingelsson M, Bergstrom J (2011) The lipid peroxidation products 4-oxo-2-nonenal and 4-hydroxy-2-nonenal promote the formation of alpha-synuclein oligomers with distinct biochemical, morphological, and functional properties. *Free Radic Biol Med* 50: 428 – 437
55. Paleologou KE, Kragh CL, Mann DM, Salem SA, Al-Shami R, Allsop D, Hassan AH, Jensen PH, El-Agnaf OM (2009) Detection of elevated levels of soluble alpha-synuclein oligomers in post-mortem brain extracts from patients with dementia with Lewy bodies. *Brain* 132: 1093 – 1101
56. Conway KA, Lee SJ, Rochet JC, Ding TT, Williamson RE, Lansbury PT Jr (2000) Acceleration of oligomerization, not fibrillization, is a shared property of both alpha-synuclein mutations linked to early-onset Parkinson's disease: implications for pathogenesis and therapy. *Proc Natl Acad Sci USA* 97: 571 – 576
57. Kim HY, Cho MK, Kumar A, Maier E, Siebenhaar C, Becker S, Fernandez CO, Lashuel HA, Benz R, Lange A *et al* (2009) Structural properties of pore-forming oligomers of alpha-synuclein. *J Am Chem Soc* 131: 17482 – 17489
58. Vinothkumar KR (2015) Membrane protein structures without crystals, by single particle electron cryomicroscopy. *Curr Opin Struct Biol* 33: 103 – 114
59. Tsigelny IF, Sharikov Y, Wrasidlo W, Gonzalez T, Desplats PA, Crews L, Spencer B, Masliah E (2012) Role of alpha-synuclein penetration into the membrane in the mechanisms of oligomer pore formation. *FEBS J* 279: 1000 – 1013
60. Fecchio C, De Franceschi G, Relini A, Greggio E, Dalla Serra M, Bubacco L, Polverino de Laureto P (2013) alpha-Synuclein oligomers induced by docosahexaenoic acid affect membrane integrity. *PLoS One* 8: e82732
61. Di Scala C, Yahi N, Boutemeur S, Flores A, Rodriguez L, Chahinian H, Fantini J (2016) Common molecular mechanism of amyloid pore formation by Alzheimer's beta-amyloid peptide and alpha-synuclein. *Sci Rep* 6: 28781
62. Lorenzen N, Nielsen SB, Yoshimura Y, Vad BS, Andersen CB, Betzer C, Kaspersen JD, Christiansen G, Pedersen JS, Jensen PH *et al* (2014) How epigallocatechin gallate can inhibit alpha-synuclein oligomer toxicity *in vitro*. *J Biol Chem* 289: 21299 – 21310
63. Liang SH, Zhang W, McGrath BC, Zhang P, Cavener DR (2006) PERK (eIF2alpha kinase) is required to activate the stress-activated MAPKs and induce the expression of immediate-early genes upon disruption of ER calcium homoeostasis. *Biochem J* 393: 201 – 209
64. Kirkpatrick CL, Wiederkehr A, Baquie M, Akhmedov D, Wang H, Gauthier BR, Akerman I, Ishihara H, Ferrer J, Wollheim CB (2011) Hepatic nuclear factor 1alpha (HNF1alpha) dysfunction down-regulates X-box-binding protein 1 (XBP1) and sensitizes beta-cells to endoplasmic reticulum stress. *J Biol Chem* 286: 32300 – 32312
65. Lampe PA, Cornbrooks EB, Juhasz A, Johnson EM Jr, Franklin JL (1995) Suppression of programmed neuronal death by a thapsigargin-induced Ca^{2+} influx. *J Neurobiol* 26: 205 – 212

66. Ghosh A, Roy A, Liu X, Kordower JH, Mufson EJ, Hartley DM, Ghosh S, Mosley RL, Gendelman HE, Pahan K (2007) Selective inhibition of NF-kappaB activation prevents dopaminergic neuronal loss in a mouse model of Parkinson's disease. *Proc Natl Acad Sci USA* 104: 18754 – 18759
67. Hunot S, Brugg B, Ricard D, Michel PP, Muriel MP, Ruberg M, Faucheux BA, Agid Y, Hirsch EC (1997) Nuclear translocation of NF-kappaB is increased in dopaminergic neurons of patients with Parkinson disease. *Proc Natl Acad Sci USA* 94: 7531 – 7536
68. Noda K, Kitami T, Gai WP, Chegini F, Jensen PH, Fujimura T, Murayama K, Tanaka K, Mizuno Y, Hattori N (2005) Phosphorylated IkappaBalpha is a component of Lewy body of Parkinson's disease. *Biochem Biophys Res Commun* 331: 309 – 317
69. Soos J, Engelhardt JI, Siklos L, Havas L, Majtenyi K (2004) The expression of PARP, NF-kappa B and parvalbumin is increased in Parkinson disease. *NeuroReport* 15: 1715 – 1718
70. Togo T, Iseki E, Marui W, Akiyama H, Ueda K, Kosaka K (2001) Glial involvement in the degeneration process of Lewy body-bearing neurons and the degradation process of Lewy bodies in brains of dementia with Lewy bodies. *J Neurol Sci* 184: 71 – 75
71. Lopez de Maturana R, Lang V, Zubiarrain A, Sousa A, Vazquez N, Gorostidi A, Aguila J, Lopez de Munain A, Rodriguez M, Sanchez-Pernaute R (2016) Mutations in LRRK2 impair NF-kappaB pathway in iPSC-derived neurons. *J Neuroinflammation* 13: 295
72. Baiguera C, Alghisi M, Pinna A, Bellucci A, De Luca MA, Frau L, Morelli M, Ingrassia R, Benarese M, Porrini V *et al* (2012) Late-onset Parkinsonism in NFkappaB/c-Rel-deficient mice. *Brain* 135: 2750 – 2765
73. Murphy KE, Gysbers AM, Abbott SK, Spiro AS, Furuta A, Cooper A, Garner B, Kabuta T, Halliday GM (2015) Lysosomal-associated membrane protein 2 isoforms are differentially affected in early Parkinson's disease. *Mov Disord* 30: 1639 – 1647
74. Nath S, Goodwin J, Engelborghs Y, Pountney DL (2011) Raised calcium promotes alpha-synuclein aggregate formation. *Mol Cell Neurosci* 46: 516 – 526
75. Lowe R, Pountney DL, Jensen PH, Gai WP, Voelcker NH (2004) Calcium (II) selectively induces alpha-synuclein annular oligomers via interaction with the C-terminal domain. *Protein Sci* 13: 3245 – 3252
76. Vogiatzi T, Xilouri M, Vekrellis K, Stefanis L (2008) Wild type alpha-synuclein is degraded by chaperone-mediated autophagy and macroautophagy in neuronal cells. *J Biol Chem* 283: 23542 – 23556
77. Lee JG, Takahama S, Zhang G, Tomarev SI, Ye Y (2016) Unconventional secretion of misfolded proteins promotes adaptation to proteasome dysfunction in mammalian cells. *Nat Cell Biol* 18: 765 – 776
78. Eichhorn EJ, Gheorghiade M (2002) Digoxin. *Prog Cardiovasc Dis* 44: 251 – 266
79. Wasserstrom JA, Aistrup GL (2005) Digitalis: new actions for an old drug. *Am J Physiol Heart Circ Physiol* 289: H1781 – H1793
80. Tuttle MD, Comellas G, Nieuwkoop AJ, Covell DJ, Berthold DA, Kloepper KD, Courtney JM, Kim JK, Barclay AM, Kendall A *et al* (2016) Solid-state NMR structure of a pathogenic fibril of full-length human alpha-synuclein. *Nat Struct Mol Biol* 23: 409 – 415
81. Martinez G, Duran-Aniotz C, Cabral-Miranda F, Vivar JP, Hetz C (2017) Endoplasmic reticulum proteostasis impairment in aging. *Aging Cell* 16: 615 – 623
82. Sacino AN, Brooks M, Thomas MA, McKinney AB, Lee S, Regenhardt RW, McGarvey NH, Ayers JI, Notterpek L, Borchelt DR *et al* (2014) Intramuscular injection of alpha-synuclein induces CNS alpha-synuclein pathology and a rapid-onset motor phenotype in transgenic mice. *Proc Natl Acad Sci USA* 111: 10732 – 10737
83. Boeve BF, Silber MH, Saper CB, Ferman TJ, Dickson DW, Parisi JE, Benarroch EE, Ahlskog JE, Smith GE, Caselli RC *et al* (2007) Pathophysiology of REM sleep behaviour disorder and relevance to neurodegenerative disease. *Brain* 130: 2770 – 2788
84. Surmeier DJ, Obeso JA, Halliday GM (2017b) Selective neuronal vulnerability in Parkinson disease. *Nat Rev Neurosci* 18: 101 – 113
85. Chan CS, Guzman JN, Ilijic E, Mercer JN, Rick C, Tkatch T, Meredith GE, Surmeier DJ (2007) 'Rejuvenation' protects neurons in mouse models of Parkinson's disease. *Nature* 447: 1081 – 1086
86. Kramer ML, Schulz-Schaeffer WJ (2007) Presynaptic alpha-synuclein aggregates, not Lewy bodies, cause neurodegeneration in dementia with Lewy bodies. *J Neurosci* 27: 1405 – 1410
87. Fortin DL, Nemani VM, Voglmaier SM, Anthony MD, Ryan TA, Edwards RH (2005) Neural activity controls the synaptic accumulation of alpha-synuclein. *J Neurosci* 25: 10913 – 10921
88. Griffiths EJ, Rutter GA (2009) Mitochondrial calcium as a key regulator of mitochondrial ATP production in mammalian cells. *Biochim Biophys Acta* 1787: 1324 – 1333
89. Bading H (2013) Nuclear calcium signalling in the regulation of brain function. *Nat Rev Neurosci* 14: 593 – 608
90. Wang QC, Zheng Q, Tan H, Zhang B, Li X, Yang Y, Yu J, Liu Y, Chai H, Wang X *et al* (2016) TMCO1 is an ER Ca(2+) load-activated Ca(2+) channel. *Cell* 165: 1454 – 1466
91. Jackson JG, Thayer SA (2006) Mitochondrial modulation of Ca^{2+} -induced Ca^{2+} -release in rat sensory neurons. *J Neurophysiol* 96: 1093 – 1104
92. Devine MJ, Gwinn K, Singleton A, Hardy J (2011) Parkinson's disease and alpha-synuclein expression. *Mov Disord* 26: 2160 – 2168
93. Goldbaum O, Oppermann M, Handschuh M, Dabir D, Zhang B, Forman MS, Trojanowski JQ, Lee VM, Richter-Landsberg C (2003) Proteasome inhibition stabilizes tau inclusions in oligodendroglial cells that occur after treatment with okadaic acid. *J Neurosci* 23: 8872 – 8880
94. Uryu K, Richter-Landsberg C, Welch W, Sun E, Goldbaum O, Norris EH, Pham CT, Yazawa I, Hilburger K, Micsenyi M *et al* (2006) Convergence of heat shock protein 90 with ubiquitin in filamentous alpha-synuclein inclusions of alpha-synucleinopathies. *Am J Pathol* 168: 947 – 961
95. Kragh CL, Fillon G, Gysbers A, Hansen HD, Neumann M, Richter-Landsberg C, Haass C, Zalc B, Lubetzki C, Gai WP *et al* (2013) FAS-dependent cell death in alpha-synuclein transgenic oligodendrocyte models of multiple system atrophy. *PLoS One* 8: e55243
96. Chesselet MF, Richter F, Zhu C, Magen I, Watson MB, Subramaniam SR (2012) A progressive mouse model of Parkinson's disease: the Thy1-aSyn ("Line 61") mice. *Neurotherapeutics* 9: 297 – 314
97. Burre J, Sharma M, Tsetsenis T, Buchman V, Etherton MR, Sudhof TC (2010) Alpha-synuclein promotes SNARE-complex assembly *in vivo* and *in vitro*. *Science* 329: 1663 – 1667
98. Gai WP, Yuan HX, Li XQ, Power JT, Blumbergs PC, Jensen PH (2000) *In situ* and *in vitro* study of colocalization and segregation of alpha-synuclein, ubiquitin, and lipids in Lewy bodies. *Exp Neurol* 166: 324 – 333
99. Jensen PH, Islam K, Kenney J, Nielsen MS, Power J, Gai WP (2000) Microtubule-associated protein 1B is a component of cortical Lewy bodies and binds alpha-synuclein filaments. *J Biol Chem* 275: 21500 – 21507
100. Gai WP, Power JH, Blumbergs PC, Culvenor JG, Jensen PH (1999) Alpha-synuclein immunoisolation of glial inclusions from multiple system

atrophy brain tissue reveals multiprotein components. *J Neurochem* 73: 2093 – 2100

101. Huang C, Ren G, Zhou H, Wang CC (2005) A new method for purification of recombinant human alpha-synuclein in *Escherichia coli*. *Protein Expr Purif* 42: 173 – 177
102. De Meis L, Hasselbach W (1971) Acetyl phosphate as substrate for Ca^{2+} uptake in skeletal muscle microsomes. Inhibition by alkali ions. *J Biol Chem* 246: 4759 – 4763
103. Meissner G, Conner GE, Fleischer S (1973) Isolation of sarcoplasmic reticulum by zonal centrifugation and purification of Ca^{2+} -pump and Ca^{2+} -binding proteins. *Biochim Biophys Acta* 298: 246 – 269
104. Gilman S, Wenning GK, Low PA, Brooks DJ, Mathias CJ, Trojanowski JQ, Wood NW, Colosimo C, Durr A, Fowler CJ *et al* (2008) Second consensus statement on the diagnosis of multiple system atrophy. *Neurology* 71: 670 – 676
105. Trojanowski JQ, Revesz T, Neuropathology Working Group on MSA (2007) Proposed neuropathological criteria for the post mortem diagnosis of multiple system atrophy. *Neuropathol Appl Neurobiol* 33: 615 – 620
106. Dickson DW, Liu W, Hardy J, Farrer M, Mehta N, Uitti R, Mark M, Zimmerman T, Golbe L, Sage J *et al* (1999) Widespread alterations of alpha-synuclein in multiple system atrophy. *Am J Pathol* 155: 1241 – 1251
107. Tao H, Lee SC, Moeller A, Roy RS, Siu FY, Zimmermann J, Stevens RC, Potter CS, Carragher B, Zhang Q (2013) Engineered nanostructured beta-sheet peptides protect membrane proteins. *Nat Methods* 10: 759 – 761
108. Suloway C, Pulokas J, Fellmann D, Cheng A, Guerra F, Quispe J, Stagg S, Potter CS, Carragher B (2005) Automated molecular microscopy: the new Leginon system. *J Struct Biol* 151: 41 – 60
109. Moller JV, Ning G, Maunsbach AB, Fujimoto K, Asai K, Juul B, Lee YJ, Gomez de Gracia A, Falson P, le Maire M (1997) Probing of the membrane topology of sarcoplasmic reticulum Ca^{2+}-ATPase with sequence-specific antibodies. Evidence for plasticity of the c-terminal domain. *J Biol Chem* 272: 29015 – 29032
110. Baginski ES, Foa PP, Zak B (1967) Microdetermination of inorganic phosphate, phospholipids, and total phosphate in biologic materials. *Clin Chem* 13: 326 – 332
111. Vilsen B, Andersen JP, Clarke DM, MacLennan DH (1989) Functional consequences of proline mutations in the cytoplasmic and transmembrane sectors of the Ca2(+)-ATPase of sarcoplasmic reticulum. *J Biol Chem* 264: 21024 – 21030